Australian Government
Department of Defence
Defence Science and
Technology Organisation

Skin-Friction Measurements on a Model Submarine

M. B. Jones, L. P. Erm, A. Valiyff and S. M. Henbest

Aerospace Division

Defence Science and Technology Organisation

ABSTRACT

Experimental skin-friction and pressure-coefficient data for a generic scale-model submarine, tested in the Low-Speed Wind Tunnel at DSTO, are presented. The effect on skin-friction and pressure coefficients due to different sizes and types of boundary layer tripping devices, including the case of no tripping device, was investigated for the Reynolds number range of 3.58×10^6 to 6.27×10^6, where the Reynolds number is based on model length. Skin friction was measured using the Preston-tube method which is a technique applicable to turbulent boundary layers only. For the laminar and transition regions the Preston tube only provided qualitative results. The results demonstrate the importance of correctly tripping the boundary layer and provide a guide on determining the size and type of tripping device required to achieve a correctly stimulated turbulent boundary layer for a given tunnel free-stream velocity. While the results are specific to the model geometry tested and for the given trip location, the methodology is applicable to other general model geometries and trip locations. This report does not address the difficult problem of where to place the trip.

APPROVED FOR PUBLIC RELEASE

APPROVED FOR PUBLIC RELEASE

Skin-Friction Measurements on a Model Submarine
Executive Summary

A series of experiments have been conducted in the Low-Speed Wind Tunnel at DSTO using a generic submarine model (1.35 m long) to investigate the effect of different boundary-layer tripping devices[1] on the skin-friction and pressure coefficients on the model. The results also provide a reference data set to assist in the development and validation of computational-fluid-dynamics codes.

The submarine model tested was in a "bare-hull" configuration aligned with the flow direction. The skin-friction was measured using a fine Pitot tube placed on the surface of the hull. A Pitot tube used in this way is referred to as a Preston tube and the technique is applicable in regions where the boundary layer is in a turbulent state. For regions where the boundary layer is laminar the Preston tube does not give quantitatively correct skin-friction values. However, the Preston tube was found to provide a useful means of determining the location of the laminar to turbulent transition point.

The results show the importance of correctly tripping the boundary layer and provide a guide for selecting the size and type of tripping device required to achieve a correctly-stimulated turbulent boundary layer, for a given wind tunnel velocity. Only a limited range of trip sizes and types were tested but it was found that a trip wire of diameter 0.2 mm or grit of size 80 give a correctly stimulated boundary layer. However, of these two devices, the wire is the preferred option since it was observed that grit may erode during a testing program. It is recommended that further work be carried out to quantify the skin friction in the laminar flow regions and the analysis be extended to other trip types such as cylindrical pins.

The location of the tripping device was fixed relative to the model and this report does not address the difficult problem of where to place the trip.

---

[1]A tripping device is used to force the boundary layer to transition from a laminar to turbulent state.

THIS PAGE IS INTENTIONALLY BLANK

Authors

Malcolm Jones
Aerospace Division

Malcolm Jones obtained a Bachelor of Engineering (Mechanical) degree in 1994 and a PhD in 1998, both from The University of Melbourne. His PhD. involved an experimental and theoretical study of a turbulent boundary layer developing in an accelerated flow. He joined the Defence Science and Technology Organisation in 2007 where he is currently employed as a Research Scientist in Aerospace Division. While at DSTO he has been involved in aerodynamic testing of aircraft models such as the F-35 and AP-3C in the Low Speed Wind Tunnel, aeroacoustic measurements and analysis of cavity flows and aerodynamic and structural measurements of flapping wings. Prior to joining DSTO he was employed as Research Fellow and then lecturer in the Department of Mechanical Engineering at The University of Melbourne (1999-2003). From 2004-2007 he worked at the School of Mathematical Sciences, Queensland University of Technology. During his academic appointments he gave lecture courses in fluid mechanics, heat transfer, manufacturing and mathematics and undertook research in turbulent boundary layer flows and biological fluid mechanics.

Lincoln Erm
Aerospace Division

Lincoln Erm obtained a Bachelor of Engineering (Mechanical) degree in 1967 and a Master of Engineering Science degree in 1969, both from the University of Melbourne. His Master's degree was concerned with the yielding of aluminium alloy when subjected to both tensile and torsional loading. He joined the Aeronautical Research Laboratories (now called the Defence Science and Technology Organisation) in 1970 and has worked on a wide range of research projects, including the prediction of the performance of gas-turbine engines under conditions of pulsating flow, parametric studies of ramrocket performance, flow instability in aircraft intakes and problems associated with the landing of a helicopter on the flight deck of a ship. Concurrently with some of the above work, he studied at the University of Melbourne and in 1988 obtained his Doctor of Philosophy degree for work on low-Reynolds-number turbulent boundary layers. Since this time, he has undertaken research investigations in the low-speed wind tunnel and the water tunnel. Recent work has been concerned with extending the testing capabilities of the water tunnel, including developing a two-component strain-gauge-balance load-measurement system for the tunnel and developing a dynamic-testing capability for the tunnel, enabling aerodynamic derivatives to be measured on models.

Aliya Valiyff
Aerospace Division

Aliya Valiyff graduated from the University of Adelaide in 2009 with a Bachelor of Aerospace Engineering and Bachelor of Science (Applied Mathematics and Physics) with 1st class honours. She commenced work with DSTO in 2010 and during her time, she has mainly worked within the Unmanned Aerial System - Corporate Enabling Research Programme (CERP), undertaking research on flapping wing and the flight and the Undersea Warfare- CERP.

Simon Henbest
Aerospace Division

Simon Henbest obtained a Bachelor of Engineering (Mechanical) degree with honours in 1977 and a PhD in 1983, both from The University of Melbourne. His PhD. titled "The Structure of Turbulent Pipe Flow" provide experimental support to Townsend's attached eddy hypothesis for wall bounded flows. In 1984 he was awarded an Australian National Research Fellowship and continued wall turbulence research at the University of Melbourne. In 1987 he commenced employment at the Aeronautical Research Laboratories (now called the Defence Science and Technology Organisation) and obtained merit promotions to both Senior Research Scientist and Principal Research Scientist. While at DSTO he has been involved in research into high speed jet and aeroacoustic cavity flows, the IR signature prediction of aircraft, numerous aerodynamic testing programmes. He has acted as a Research Leader for extended periods in AVD, AOD and HPPD. He is currently Head of Fluid Mechanics in Aerospace Division.

THIS PAGE IS INTENTIONALLY BLANK

Contents

Appendices

Glossary

DARPA	Defense Advanced Research Projects Agency
CERP	Corporate Enabling Research Program
CFD	Computational Fluid Dynamics
LSWT	Low-Speed Wind Tunnel
DSTO	Defence Science and Technology Organisation

Notation

C_f	Local skin-friction coefficient
C_p	Pressure coefficient
d	Outer diameter of Preston tube
d_T	Diameter of trip wire
h	Height of grit transition strip
p_∞	Free-stream static pressure
p_p	Total pressure of Preston tube
p_s	Model surface static pressure
p_t	Free-stream total pressure
p_x^+	Non-dimensional pressure gradient parameter
Re	Reynolds number
Re_{d_T}	Reynolds number based on diameter of wire
Re_x	Reynolds number based on the stream-wise coordinate
Re_{x_t}	Streamwise Reynolds number of transition point
U	Streamwise velocity in boundary layer
U_1	Streamwise velocity at edge of boundary layer
U_∞	Nominal streamwise velocity in tunnel working-section
U_τ	Friction velocity
w	Width of grit transition strip
x	Streamwise coordinate
x_t	Streamwise coordinate of transition point
y	Wall normal coordinate
Δp	$\Delta p = p_p - p_s$
ν	Kinematic viscosity
ρ	Fluid density
τ_0	Wall shear stress

THIS PAGE IS INTENTIONALLY BLANK

1   Introduction

This work aims to understand flow fields about a submarine. As part of this program, a series of experiments have been conducted in the Low-Speed Wind Tunnel (LSWT) at the Defence Science and Technology Organisation (DSTO) to quantify the skin-friction distributions on a generic submarine model and in the process investigate the effectiveness of a limited range of tripping devices. The results also provide a reference data set for computational fluid dynamics (CFD) validation of a submarine model.

When conducting tests in wind tunnels on a sub-scale model, for results of the experiment to be transferable to the full-scale vehicle, the flow patterns and load coefficients on the model and the full-size vehicle need to be made similar. Ideally, this is achieved through matching the Reynolds number of the flow over the model to that of the full-scale vehicle. However, in practice this is difficult to achieve and is not always possible. To ensure that the flow features on the model are representative of those for the full-size vehicle, a tripping device can be used such that the boundary layers (i.e. regions of laminar flow, laminar-to-turbulent transition and turbulent flow) are made similar. However, different tripping devices can impart different disturbances into the flow. In order to correctly stimulate the boundary layer on the submarine model and avoid over- or under-stimulation, the type and size of tripping devices need to be selected for a given Reynolds number or Reynolds number range and also for a specific trip location. Additionally, the chosen tripping device will be specific to a given tunnel and would be dependent on factors such as the level of free-stream turbulence in the tunnel.
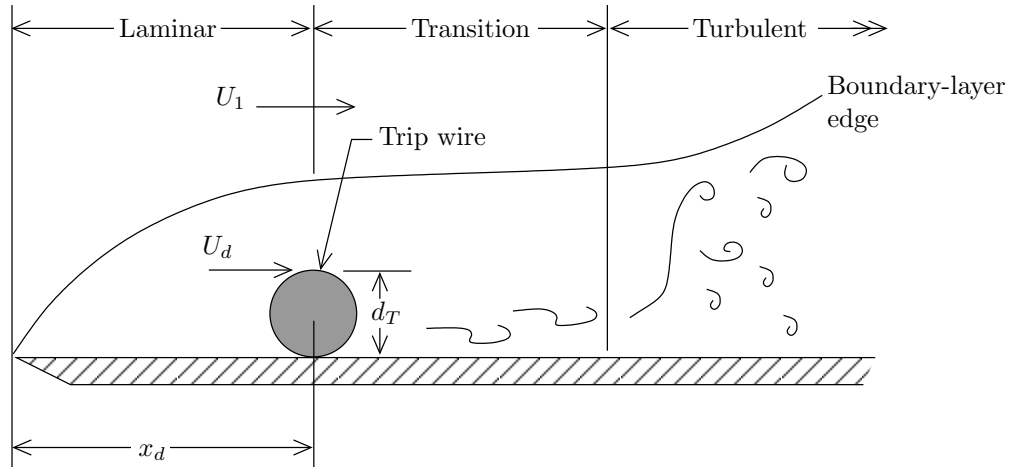
Figure 1: *Diagrammatic representation of a boundary layer being tripped, based on a diagram given by White (1974)*

1.1   Boundary-Layer Transition

Boundary-layer transition is a complicated physical process dependent on instability mechanisms, including Tollmien-Schlichting waves, crossflow and Gortler instabilities (see Reed & Saric, 2008). Over the years, there have been numerous articles published on transition, both from experimental investigations and CFD analyses, in low-speed, transonic

and hypersonic flow regimes (for example Schlatter & Henningson, 2009). Details of the transition process are still not fully understood. In the present report, transition physical processes are not considered, instead attention is focused on how to stabilise the position of the transition using a tripping device and to ensure that the turbulent boundary layer is neither under- or over-stimulated, irrespective of the flow physics associated with transition.

1.2   Approach of Erm & Joubert (1991)

A diagrammatic representation of a boundary layer being tripped is shown in Figure 1, where d_T is the height of the tripping device, U_1 is the streamwise velocity at the edge of the boundary layer, x_d is the location of the tripping device measured from the nose of the model and U_d is the velocity in the boundary layer at the top of the device.

A question that had to be addressed was what is the best size and type of tripping device to use in the current experiments in the LSWT to trip the boundary layer on the submarine model. Erm & Joubert (1991) faced a similar question in their studies on low-Reynolds-number flows over a smooth flat surface in a zero pressure gradient. For different types of tripping devices, they measured longitudinal skin-friction coefficients for a range of free-stream velocities. Their data for a 1.2 mm wire tripping device are reproduced in Figure 2. From this figure it can be seen that as the velocity is increased from 8 m/s, the device imparts an increased amount of turbulent energy into the flow so that the laminar-to-turbulent transition region moves upstream. They conjectured that correct stimulation is associated with a particular curve when the peaks of successive curves, corresponding to higher velocities, do not advance significantly upstream. Velocities lower than that corresponding to the particular curve were obviously associated with under-stimulated flows since the peaks of the curves were well downstream of the device and thus the device was therefore not completely effective in tripping the flow. Since the velocity corresponding to the particular curve establishes a turbulent boundary layer almost to the possible upstream limit of turbulent flow, it seemed reasonable to assume that the main effect of higher velocities was to overstimulate the flow.

The x-coordinate corresponding to the peaks of Figure 2 are plotted in Figure 3 as a function of streamwise velocity and it is apparent that the above condition for correct stimulation was satisfied when the velocity was between 10 and 12 m/s. This corresponds to a minimum Reynolds number of the tripping device in the range of $Re_{d_T} = U_1 d_T/\nu = 800$ to 960, where ν is the kinematic viscosity. For the case where a trip device has a Reynolds number greater than the minimum required, the tripping device may overstimulate the flow. Note, over-stimulation does not necessarily result in higher skin-friction when compared to a correctly stimulated layer. Rather it means that the disturbance introduced by the tripping device is felt downstream of the transition region and leads to a "non-standard" turbulent boundary initially developing. Ideally, to assess whether over-stimulation has occurred, complete velocity profiles in the turbulent region need to be measured and compared against reference data sets such as those collated by Coles (1962).

It should be noted that in the current work, the boundary layer develops in a pressure gradient with wall curvature in both the streamwise and spanwise directions. Whereas

the work of Erm & Joubert (1991) was undertaken on a flat plate zero pressure gradient, this means the Re_{d_T} values given above cannot be applied directly to predict the trip size required. However the approach taken here broadly follows that of Erm & Joubert (1991), in that, a range of trip Reynolds numbers were tested (by varying both freestream velocity and trip size) and the skin-friction downstream of the trip measured.
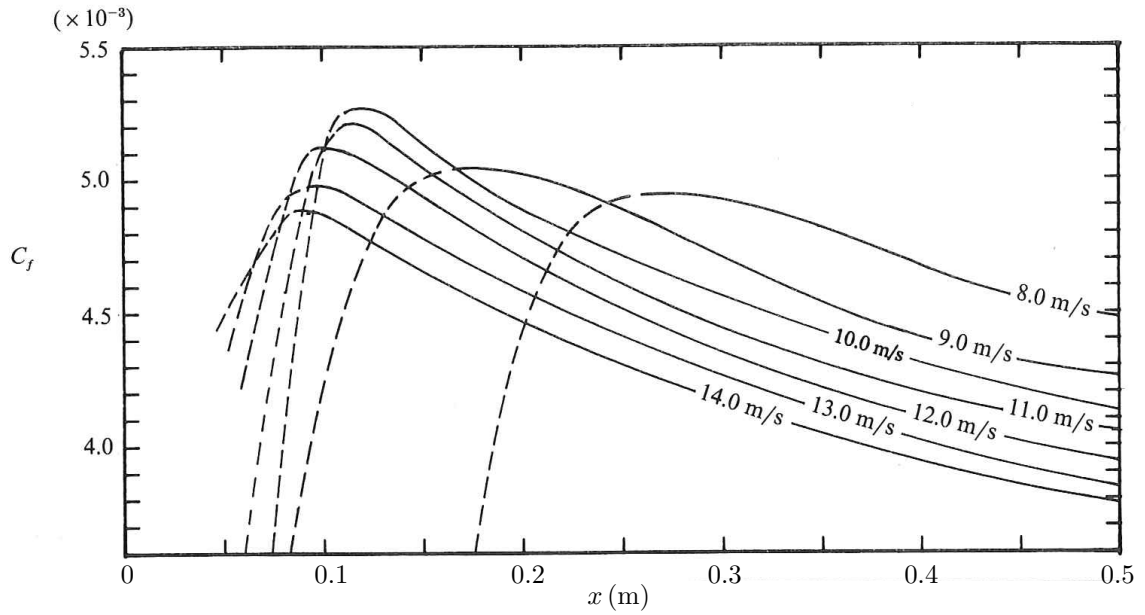

Figure 2: C_f *vs* x *measurements for a* $1.2\,mm$ *diameter trip wire for different free-stream velocities, as obtained by Erm & Joubert (1991).*
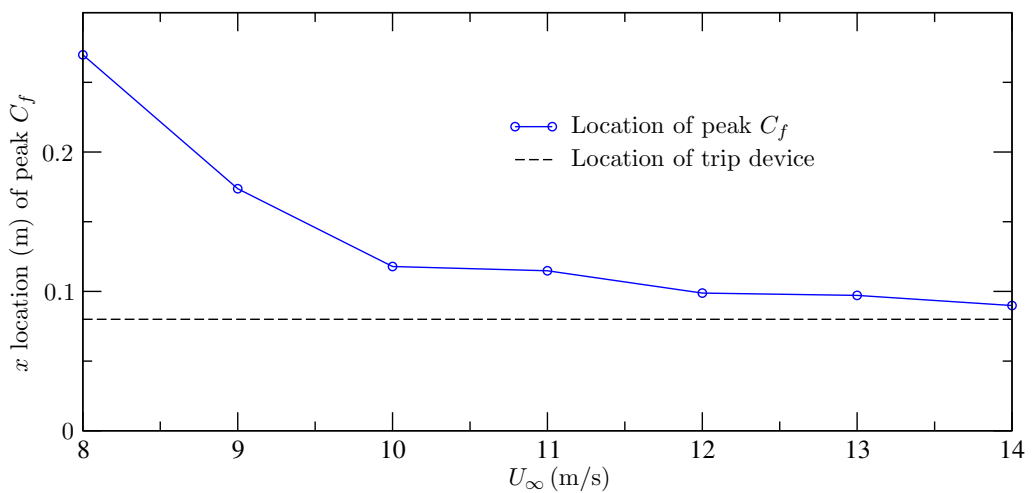

Figure 3: *Location of the peak* C_f *values shown in Figure 2.*

1.3   Empirical Expressions to Determine Sizes of Tripping Devices

Researchers have proposed different empirical expressions for determining the size of device to use to trip the flow. The relationships incorporate parameters including the height of the tripping device, d_T, the velocity at the edge of the boundary layer, U_1, the velocity in the undisturbed boundary layer at the top of the device, U_d, and the wall friction velocity evaluated at the device, U_τ. The friction velocity is defined by $\tau_0 = \rho U_\tau^2$ where τ_0 is the surface shear stress and ρ is the fluid density. Recommendations for fully-effective tripping cover quite a wide range. Tani *et al.* (1940) proposed the criterion $U_\tau d_T/\nu = 13$, Fage & Preston (1941) proposed $U_\tau d_T/\nu = 20$, Braslow & Knox (1958) proposed $U_d d_T/\nu = 600$ and Gibbings (1959) proposed $U_1 d_T/\nu = 826$. It should be noted that, the criterion of Gibbings (1959) is based on a review of many data sets included those of Tani & Sato (1956) and Fage & Preston (1941). Gibbings (1959) expresses the Tani & Sato (1956) and Fage & Preston (1941) criteria as Reynolds numbers based on the freestream velocity, which gives values of $U_1 d_T/\nu = 600$ and 840 respectively. The criterion given above represent minimum values of the tripping device Reynolds number, required to correctly trip the boundary layer and agree with the results of Erm & Joubert (1991).

An analysis of the literature for tests done on bodies of revolution indicated that there is no consistent approach for selecting the size and type of device to use on such bodies. Appendix A gives details of devices used by different investigators for bodies of revolution, together with other experimental information. Based on the freestream velocity and trip height, the Reynolds numbers of the trip devices given in Appendix A range from 200 to 40×10^3. For the present investigation, the approach used to establish the effects that different devices had on tripping laminar boundary layers was similar to that used by Erm & Joubert (1991) for a smooth flat plate in a zero pressure gradient. Using their technique, it is possible to establish the size and type of tripping device to be used for a given velocity to obtain correctly stimulated turbulent boundary layers.

2   Preston-Tube Method of Measuring Skin-Friction Coefficients

Skin-friction coefficients in a turbulent boundary layer flowing over a smooth surface can be measured in a number of different ways (Fernholz *et al.*, 1996), including using Preston tubes (Preston, 1954), from velocity profiles and using devices mounted flush with the surface of a model. Of the alternative approaches, the Preston-tube method is convenient and is widely used. The method makes use of a simple Pitot tube placed on the surface of a body and when used this way it is termed a Preston tube. The method depends on an underlining assumption that in the region adjacent to the surface the flow is primarily determined by the surface shear stress and the properties of the fluid and is independent of factors such as pressure gradient and surface curvature. The assumption implies that the velocity profile in a turbulent boundary layer adjacent to the surface is given by

$$\frac{U}{U_\tau} = f\left(\frac{U_\tau y}{\nu}\right) \tag{1}$$

where U is the local stream-wise velocity, U_τ is the friction velocity, f is a universal function, y is the wall normal coordinate and ν is the kinematic viscosity. Equation (1) is often referred to as the "law of the wall" (Coles, 1956).

A Pitot tube placed on the wall will measure a pressure, relative to the wall static pressure, of $\Delta p = \rho U^2 / 2$, at an effective coordinate $y = c_0 d$, where d is the outer diameter of the Pitot tube and c_0 is an unknown constant. Substituting the values $U = \sqrt{(2\Delta p/\rho)}$ and $y = c_o d$ into (1) yields a relationship between the wall shear stress, fluid properties, Preston-tube pressure difference, and the tube diameter, which is given by

$$\frac{2\Delta p}{\rho U_\tau{}^2} = \left[f\left(\frac{U_\tau c_0 d}{\nu} \right) \right]^2 . \tag{2}$$

Alternatively, for the purpose of measuring skin friction, (2) can be expressed more conveniently in the form

$$\frac{\tau_0 d^2}{4\rho\nu^2} = F\left(\frac{\Delta p d^2}{4\rho\nu^2} \right) \tag{3}$$

where c_0 has been absorbed into the function F. The function F represents the "calibration" function for a Preston tube and several experimentally derived forms exist in the literature (see Preston, 1954; Patel, 1965; Zagarola *et al.*, 2001). Generally the calibration is determined by placing the Preston tube in a pipe flow where the wall shear stress (or friction factor) can be determined accurately by measuring the pressure gradient in the pipe.

For the data presented in this report, the calibration of Patel (1965) was used to determine the wall shear stress. The calibration curve of Patel (1965) is given as follows:

$$x^* = y^* + 2\log_{10}(1.95 y^* + 4.10), \qquad \text{for } 55 < \frac{U_\tau d}{2\nu} < 800; \tag{4}$$

$$y^* = 0.8287 - 0.1381 x^* + 0.1437 x^{*2} - 0.006 x^{*3}, \qquad \text{for } 5.6 < \frac{U_\tau d}{2\nu} < 55 \text{ and} \tag{5}$$

$$y^* = \frac{1}{2} x^* + 0.037, \qquad \text{for } \frac{U_\tau d}{2\nu} < 5.6 \tag{6}$$

where

$$x^* = \log_{10}\left(\frac{\Delta p d^2}{4\rho\nu^2} \right) \qquad \text{and} \qquad y^* = \log_{10}\left(\frac{\tau_0 d^2}{4\rho\nu^2} \right) .$$

The local skin friction coefficient C_f is then found using

$$C_f = \frac{\tau_0}{\frac{1}{2}\rho U_1^2} \tag{7}$$

where U_1 is the streamwise velocity at the edge of the boundary layer.

The calibration given by (4)-(6) is valid only for a *hydrodynamically smooth* surface. A surface is considered hydrodynamically smooth provided that the height of surface roughness elements remain less than $5\nu/U_\tau$ (Jimenez, 2004). The minimum value of $5\nu/U_\tau$ that was measured was approximately $4\,\mu\text{m}$ and the measured surface finish was found to be an order of magnitude less than this value (Section 3.2). Hence, the requirement of a hydrodynamically smooth surface is satisfied for this experiment.

The fundamental requirement for using a Preston tube is that the boundary layer is in a turbulent state and that the dimension of the Preston tube is such that it remains within the region where (1) is valid (i.e. from (4) $U_\tau d/\nu < 1600$). The diameter of the Preston tube for all experiments was $d = 0.6\,\text{mm}$ and this ensured that $U_\tau d/\nu$ remained less than 1600, well within the range of the calibration (4).

It is known that for sufficiently strong pressure gradients the form of (1) changes (see Nickels, 2004). Patel (1965) quantifies the effect of pressure gradients using the non-dimensional pressure gradient parameter[1]

$$p_x^+ = \frac{\nu}{\rho U_\tau^3}\frac{dp}{dx}.$$

(8)

The error associated with using a Preston tube in pressure gradients is quantified by Patel (1965) and is given by the following inequalities

1. Adverse pressure gradient

$$\text{Max Error } 3\%:\ 0 < p_x^+ < 0.01 \text{ and } \frac{U_\tau d}{\nu} \leq 200,$$

(9a)

$$\text{Max Error } 6\%:\ 0 < p_x^+ < 0.015 \text{ and } \frac{U_\tau d}{\nu} \leq 250.$$

(9b)

2. Favourable pressure gradient

$$\text{Max Error } 3\%:\ -0.005 < p_x^+ < 0 \text{ and } \frac{U_\tau d}{\nu} \leq 200,\ d/dx(p_x^+) < 0$$

(10a)

$$\text{Max Error } 6\%:\ -0.007 < p_x^+ < 0 \text{ and } \frac{U_\tau d}{\nu} \leq 200,\ d/dx(p_x^+) < 0.$$

(10b)

The pressure gradient data are presented in Section 4.4 and were found to fall within the limits of (9a) and (10a), indicating that the skin-friction coefficients are valid to within $\pm 3\,\%$. This accuracy is similar to the alternative direct skin-friction measuring techniques which typically achieve an accuracy of $\pm 4\,\%$ (Fernholz *et al.*, 1996).

The effect of model spanwise curvature on (4)-(6) is not quantified. A reasonable assumption is that since the boundary layer thickness is much less than the model diameter the effect of spanwise model curvature can be neglected.

The Preston-tube method, as outlined above, requires that the boundary layer is in a turbulent state. For this reason the method cannot be used to infer the skin friction at locations were the boundary layer is in a laminar state. However, the Δp values read by the Preston tube can be used to determine where laminar-to-turbulent transition occurs. The region of transition is associated with a discontinuity in Δp, when plotted as a function of streamwise coordinate x, as shown by Erm & Joubert (1991).

---

[1]for clarity we have adopted the notation for the pressure gradient parameter used by Nickels (2004), Patel (1965) uses the symbol Δ.
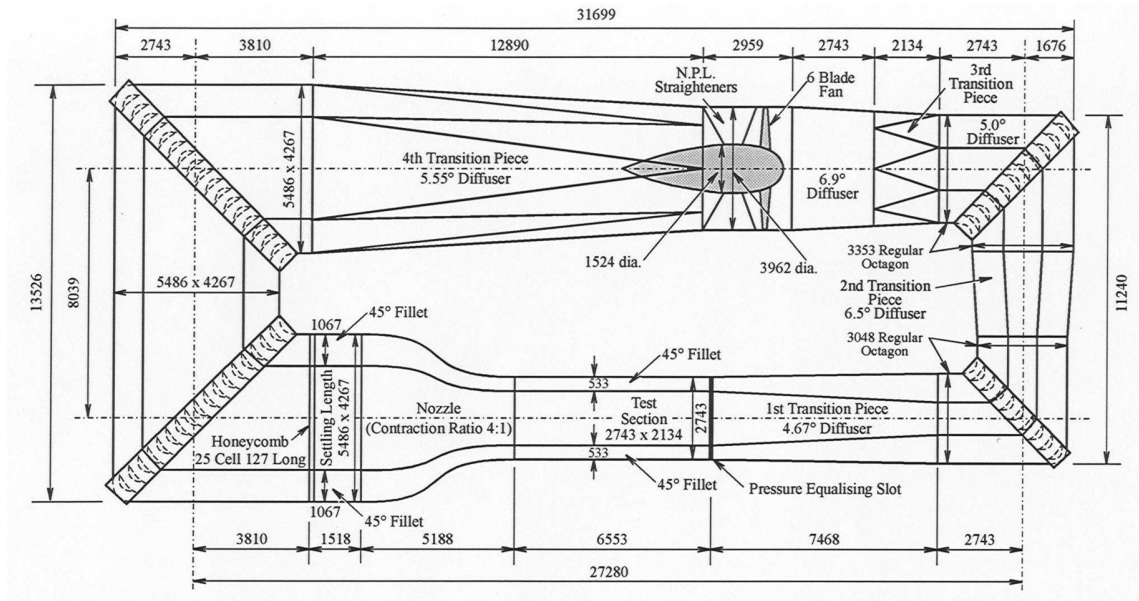
Figure 4: LSWT Layout, see Erm (2003).

3   Test Program

In this preliminary investigation, four different tripping devices were used to investigate the effect of the device on the skin-friction profile of a generic sub-scale submarine model. Tests were conducted both with and without the tripping devices at a range of nominal free-stream velocities, U_∞, ranging from $U_\infty = 40$ to $70\,\mathrm{m/s}$ to assess their effectiveness in tripping the boundary layer.

3.1   Test Facility

The Low-Speed Wind Tunnel at DSTO is a closed circuit continuous flow tunnel with a contraction ratio of 4:1. The test section has an irregular octagonal shape with a height of 2.13 m, a width of 2.74 m and a length of 6.553 m, with a longitudinal turbulence intensity of approximately 0.4% in the region where the models are tested (see Erm, 2003). An outline of the plan of the wind tunnel is shown in Figure 4. Free-stream velocities were measured using static pressure rings at the upstream and downstream ends of the contraction. A Pitot-static probe, mounted on the side wall near the front of the working section, was used to provide an independent measurement of the free-stream velocity.

3.2   Test Model

The sub-scale submarine model utilised in these tests is referred to as the *Joubert model* since the geometry is based on the work of Joubert (2004) and Joubert (2006) as well as Loid & Bystrom (1983). The model was designed for the purpose of experimental and
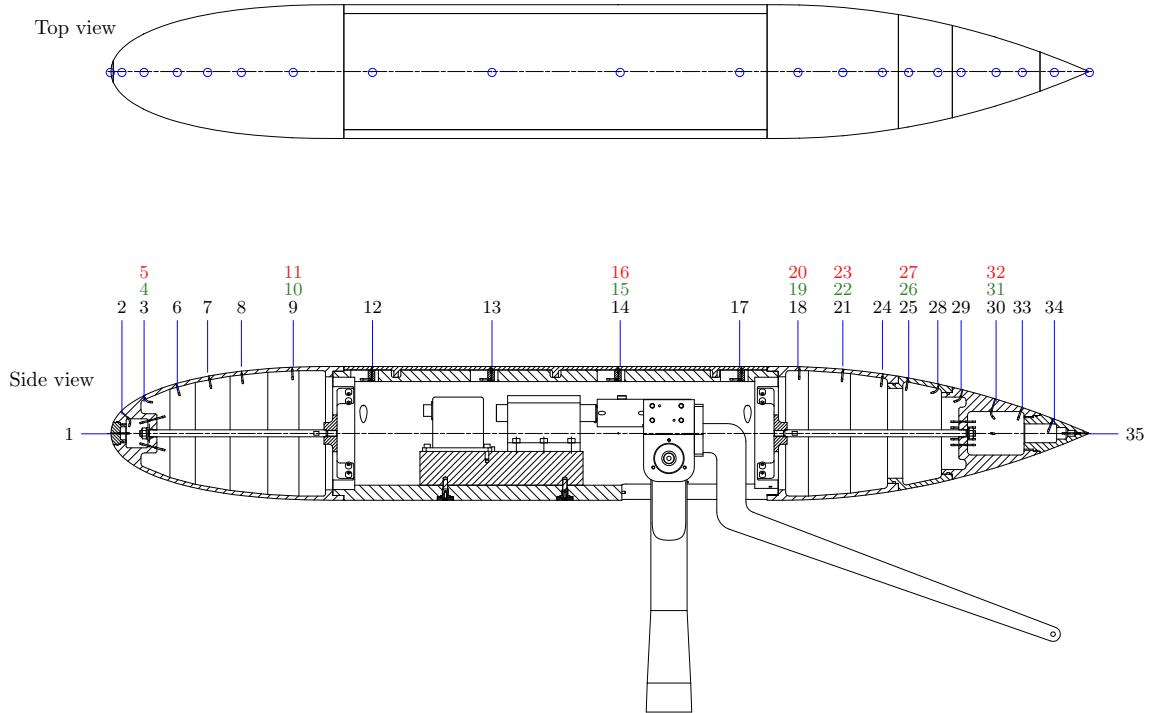
Figure 5: *Schematic of scale model showing static-pressure port locations, green and red markers represent the starboard and port static-pressure ports, respectively.*

numerical studies and has no full-scale equivalent. While the full model includes a casing, centre fin and control surfaces, all tests reported here were conducted on the axisymmetric body shape only.

The model was machined from aluminum and consists of an ellipsoidal nose, a cylindrical centre-body and a streamlined tail section. At the design stage, an N6 surface finish was specified for the model, which corresponds to a roughness of $0.8\,\mu$m in waviness. After manufacture, the surface finish was checked using a *Surface Roughness Indicator*, and the finish was found to be better than the design specification. The model was anodised, which increased the thickness of the natural oxide layer by about $10\,\mu$m.

The model is $1350\,$mm long with a maximum diameter of $185\,$mm and slenderness ratio of 7.3, where the slenderness ratio is defined as hull length divided by maximum hull diameter. The model contains 21 longitudinal static-pressure ports on the centre-line of the upper surface and 14 lateral static-pressure ports offset to the port and starboard sides of the upper surface centre-line. Figure 5 shows the stream-wise location of the static-pressure ports.

The model was supported by a single pylon as shown in Figure 6. All tests were carried out at zero angle of yaw and zero angle of pitch. The origin of the body coordinate system is located at the nose of the submarine model. The x-axis corresponds to the axis of symmetry of the model.

Figure 6: *Submarine model mounted in LSWT, showing pylon support and pitch control arm.*

Table 1: *Details of tripping devices, where the Reynolds number is based on the height of the device. The minimum Reynolds number and maximum Reynolds number correspond to nominal freestream velocities of $U_\infty = 40\,m/s$ and $U_\infty = 70\,m/s$ respectively, where h is the height of the grit and w is the width of the grit.*

Device	Dimensions (mm)	Re_{d_T} (min.)	Re_{d_T} (max.)
Wire 1:	$d_T = 0.1$	281	496
Wire 2:	$d_T = 0.2$	577	1015
Wire 3:	$d_T = 0.5$	1443	2566
80 Grit:	$h = 0.21,\ w = 3$	605	1073

3.3 Tripping Devices

In this work, four tripping devices were tested and consisted of circular wires with diameters $d_T = 0.1$, 0.2 and $0.5\,$mm, as well as a distributed silicon carbide grit of size 80, having a width of $3\,$mm. The circular wires were bent to conform to the local diameter of the submarine and then attached with "super-glue" such that there was no gap between the wire and the model surface, Figure 7. The silicon carbide grit is prepared by distributing a layer of grit on double-sided sticky tape, the tape is then adhered to the submarine, Figure 8. The tripping devices were attached to the submarine model circumferentially, located at a streamwise coordinate of $x = 67.5\,$mm measured from the nose of the submarine, which corresponds to 5% of the total model length. The dimensions of the trip devices, along with the Reynolds number range of the trip devices, are summarised in Table 1. Note that the Reynolds number of the trip device is defined as $Re_{d_T} = U_1 d_T / \nu$ where for the case of the 80 grit d_T is replaced by the grit height h.

3.4 Pressure Scanners

Pressure Systems Incorporated (PSI) brand pressure scanners were used to measure all static and total pressures. The pressure scanners are differential pressure measurement units consisting of an array of silicon piezoresistive pressure sensors, one for each pressure port. The outputs of the sensors are electronically multiplexed through a single on-board instrumentation amplifier using binary addressing. The scanners include a two-position calibration manifold actuated by momentary pulses of control pressures. In the calibrate position, all sensors are connected to a common calibration pressure port. A series of accurately-measured pressures is applied through this port to characterize the sensors. Proper and periodic on-line calibration maintains static errors within $\pm 0.03\,\%$, or better, of the full-scale pressure range.

The pressure scanners are controlled and sampled using a PSI 8400 electronic measurement system. It is a modular, parallel processing system for high-speed pressure scanning at up to 20,000 measurements per second and allows the use of digitally temperature compensated pressure scanners.

Two differential pressure scanners were used in the experiments. All pressures are measured relative to the free-stream static pressure, p_∞, as measured by the reference free-stream Pitot-static probe. Each pressure scanner contained 32 ports. The full-scale
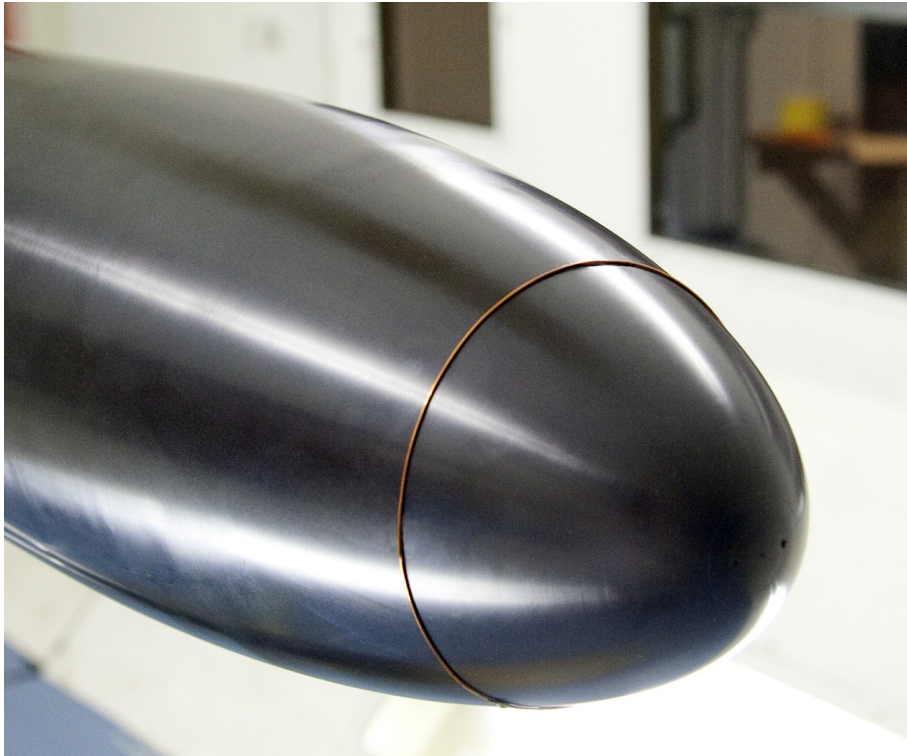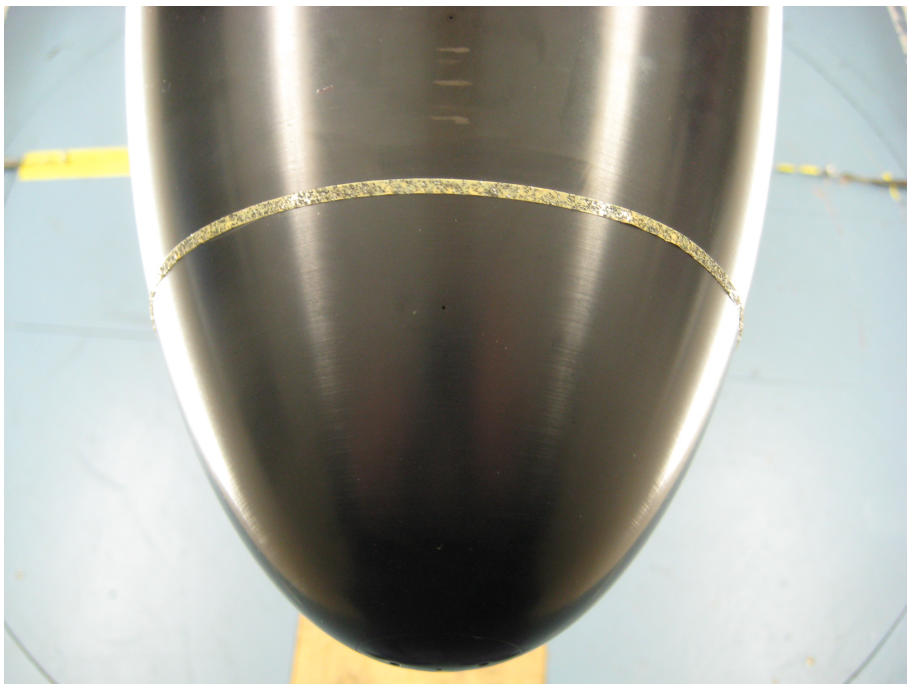
Figure 7: *Location of trip wire.*

Figure 8: *Photo showing the 3 mm wide band of 80 grit transition strip.*

pressure range of the scanners is 2.49 kPa ("10 inches-of-water scanner") and 6.89 kPa ("1 psi scanner"). The 6.89 kPa scanner was used to read the static pressure at the longitudinal ports as well as the output from the Preston tube and the Pitot-static probe.

For the purpose of cross-checking and for redundancy the Preston tube was connected to two independent ports of the 6.89 kPa scanner and the two readings averaged. For this scanner, pressures could be read to an accuracy of 6890×0.0003 Pa, i.e. about 2 Pa. The minimum Δp measured by the Preston tube was 145 Pa, which gives a pressure scanner resolution of 1.4 %. However, this minimum Δp was recorded for a location where the Preston tube was in a laminar boundary layer and such data is only useful in a qualitative sense (see Section 2). For locations were the boundary layer is turbulent the minimum Δp was 340 Pa, which gives a pressure scanner resolution of 0.6 %. The 2.49 kPa scanner was used mainly to acquire the static pressures at the lateral ports.

3.5   Data Acquisition Software

A software package called ImPressOne was used which communicates with the PSI 8400 and displays and acquires the pressure data for the model under test. For the static pressure measurements, 100 readings were acquired at each pressure port at a sampling rate of 20 Hz. For the Preston-tube measurements, the sample rate was increased and 100 samples were acquired at each pressure port at a sampling rate of 50 Hz for each free-stream velocity.

3.6   Experimental Procedure

The hull was tested with each of the selected tripping devices listed in Table 1, as well as without a tripping device, resulting in five different test configurations. For each test configuration, the static pressures were initially acquired for that particular configuration followed by the Preston-tube measurements.

A Preston tube having a diameter of 0.6 mm was attached to the surface of the model using both plasticine and tape to ensure that the tube was positioned as flat as possible on the surface of the model as shown in Figure 9. Preston-tube measurement were taken on the upper surface of the submarine model, along a line directly above the centre-line of the model. For the $d_T = 0.2$ and 0.5 mm wires and the grit case, measurements were taken from $x = 73$ mm to $x = 1065$ mm, for a total of 18 stations. For the $d_T = 0.1$ mm wire, measurements were limited to 3 stations between $x = 305$ mm and $x = 442$ mm. The stream-wise coordinates for the Preston tube measurements are given in the Table 2. Data were acquired for a range of free-stream velocities from 40 to 70 m/s in increments of 5 m/s.

For each nominal velocity, the corresponding model Reynolds number was calculated assuming standard temperature and atmospheric pressure conditions, $20°$ C and $101,325$ Pa respectively. For each given test, the temperature and static pressure of the air within the test section were logged and the air density and viscosity were calculated. To account for daily variations in temperature and atmospheric pressure, the freestream
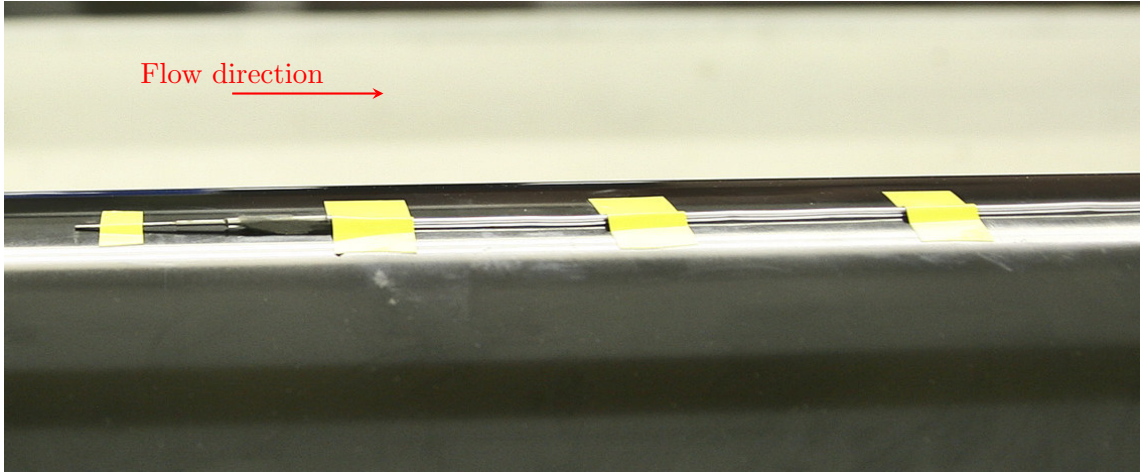
Figure 9: *Preston tube located on the centre-line of the upper-surface of submarine.*

velocity was adjusted to ensure that the model Reynolds number remained constant for each given nominal velocity condition, as shown in Table 3.

Table 2: *Skin-friction measurement stations. Where applicable, the corresponding static port number is given. For the $d_T = 0.1\,mm$ wire, measurements were only taken at stations 305.0, 360.0 as well as an additional station at $x = 442.5\,mm$*

x mm	73.1	78.7	84.3	90.0	112.5	135.0	157.5	180.0	215.0
Static port	-	-	-	6	-	7	-	8	-
x mm	250.0	305.0	360.0	525.0	700.0	870.0	950.0	1010.0	1065.0
Static port	9	-	12	13	14	17	18	21	24

Table 3: *Reynolds numbers (based on submarine length, $1.35\,m$) corresponding to the nominal free-stream velocities.*

Nominal U_∞	40	45	50	55	60	65	70	m/s
Re	3.58	4.03	4.48	4.93	5.37	5.82	6.27	$\times 10^6$

3.7   Data Reduction

The static pressure readings from the pressure ports were converted to pressure coefficients using the relationship

$$C_p = \frac{p_s - p_\infty}{p_t - p_\infty} \tag{11}$$

where p_∞ is the reference free-stream static pressure, p_t is the reference free-stream total pressure and p_s is the static pressure on the surface of the submarine model.

As explained in Section 3.4, all Preston tube pressures are measured relative to the free-stream static pressure. In order to apply the Preston tube calibration (4)-(6), the logged Preston-tube pressure differences (i.e. $p_p - p_\infty$) must first be converted to a $\Delta p = p_p - p_s$

pressure difference, where p_p is the Preston tube total pressure. In order to convert the Preston pressure differences to Δp values, C_p data obtained without a Preston tube on the surface are used. The conversion is then given by

$$\Delta p = \underbrace{(p_p - p_\infty)}_{\text{current}} - \underbrace{C_p}_{\text{prior}} \underbrace{(p_t - p_\infty)}_{\text{current}}, \tag{12}$$

where "current" indicates data logged during the Preston-tube measurement and "prior" indicates data logged during the pressure-port measurements. For stream-wise coordinates where there is no static pressure port, the C_p data were interpolated using a cubic spline. An example of a cubic spline fit to the C_p data is given in Figure 10 for the case of $U_\infty = 70\,\text{m/s}$ with the $d_T = 0.5\,\text{mm}$ trip wire. While the spline is a reasonable fit, inspection of Figure 10 suggests a greater density of static pressure ports should be used in future measurements.

A C-language computer program was written to process the Preston-tube data and details of this program are given in Appendix B.
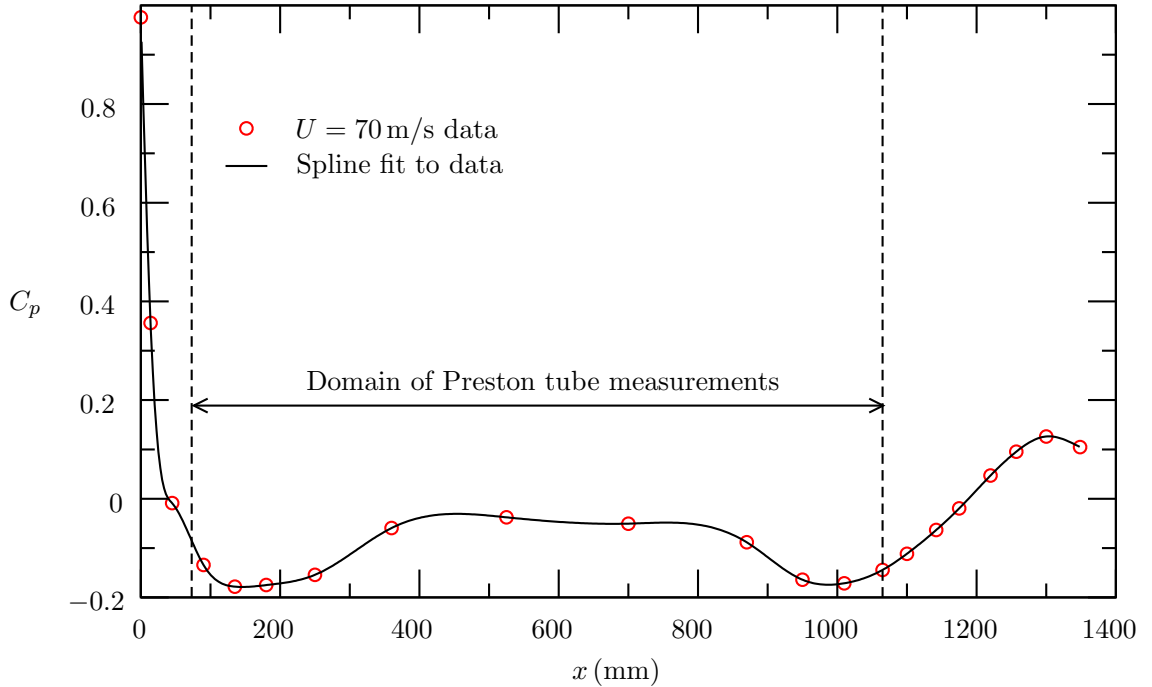
Figure 10: *Example of a cubic spline fit to C_p data, showing domain of Preston-tube data. Data is shown for the case of $U_\infty = 70\,m/s$ with the $d_T = 0.5\,mm$ trip wire.*

4 Results

4.1 Skin Friction Without a Tripping Device

Figure 11 shows the skin friction results as a function of stream-wise coordinate for the case of no tripping device. Care must be taken in interpreting the data for the no-tripping-

device case. As explained in Section 2, a Preston tube can measure skin friction provided the boundary layer is:

1. in a fully turbulent state,

2. the Preston tube is within the universal region of the boundary layer and

3. the strength of the pressure gradient does not effect the universal region of the boundary layer velocity profile.

For the case of no tripping device, the boundary layer is initially laminar and at some stream-wise coordinate natural transition occurs. As a consequence the C_f values inferred by the Preston tube in the regions upstream of transition are incorrect, owing to the fact that a universal turbulent region does not exist. The data for these regions are marked by the dashed curves in Figure 11 and quantitatively the data are of no use for the purpose of estimating the skin friction. However, qualitatively the data corresponding to laminar flow and transitioning flow can be used to estimate the point of transition, which occurs at the local minimum of the dashed curves in Figure 11.
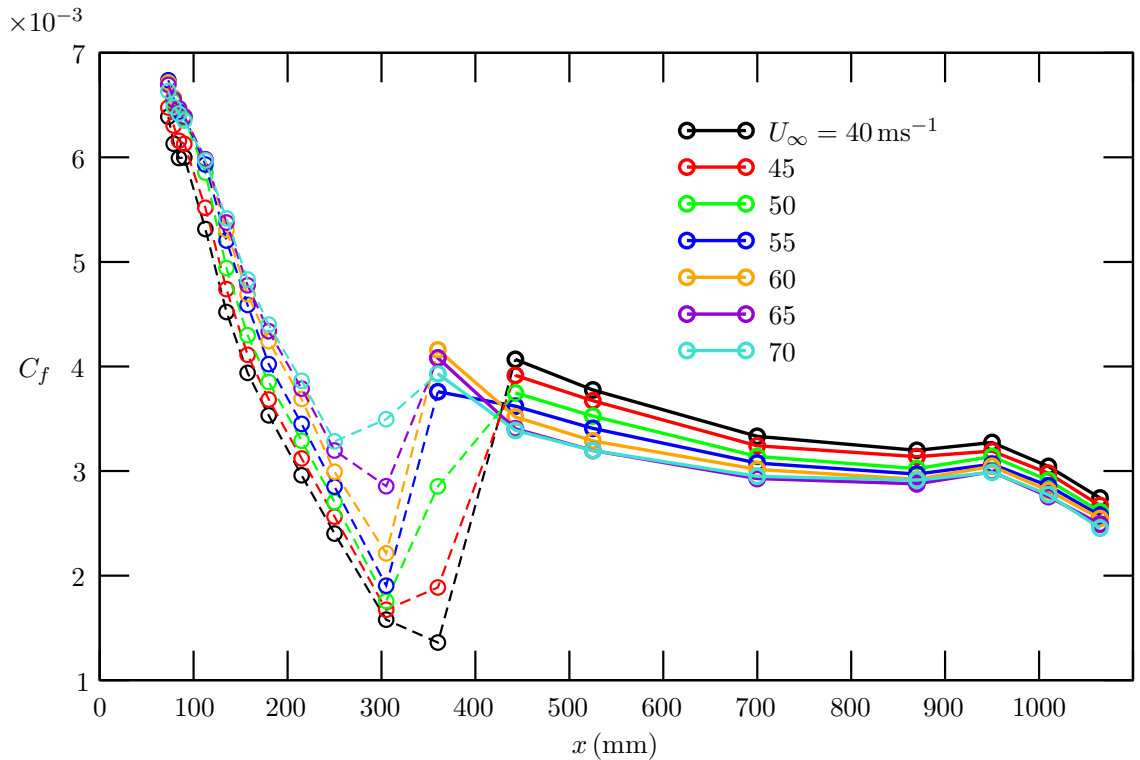
Figure 11: *Skin friction development without tripping device. Dashed lines indicate data were obtained in a laminar or transitioning profile and in these regions the Preston tube method breaks down. Only the data shown by the bold curves is quantitatively valid.*

To estimate the transition point, a cubic function is fitted about the local minimum of the curves in Figure 11. The minimum of the cubic curve fit is then used to estimate the transition point. The estimates of the transition point are given in Table 4 for the

range of free-stream velocities. For the lowest measured velocity, the transition point, x_t, was found to be about 340 mm from the nose of the submarine model. As expected, the transition point moved upstream with increasing velocity and for the highest measured velocity the transition point was located at about 260 mm. The trend of the transition point with tunnel free-stream velocity indicates that transition is occurring "naturally" and is not being initiated by any surface imperfections. The local Reynolds number, based on the stream-wise coordinate at transition, varies between $R_{x_t} = 0.91 \times 10^6$ to $R_{x_t} = 1.22 \times 10^6$ across the free-stream velocity range of the experiments. It is possible that the R_{x_t} variation is partially due to the error associated with estimating the transition point using spatially sparse data and it is recommended that for future work, measurements are taken at more closely spaced streamwise stations in the transition region.

Table 4: *Estimate of transition point and transition Reynolds number based on Preston-tube results.*

U_∞ (m/s)	40	45	50	55	60	65	70
x_t (mm)	343	330	291	306	302	295	263
Re_{x_t} ($\times 10^6$)	0.910	0.985	0.966	1.12	1.20	1.27	1.22

4.2   Skin Friction With Tripping Devices

Skin friction coefficients over the submarine model for the case of trip wires with diameters of 0.2 mm and 0.5 mm as well as for 80 grit are given in Figures 12, 13 and 14 respectively. These data, as well as data for the case of no tripping device, are given in Appendix C, where data are plotted for each test velocity.

Figures 12 to 14 indicate that the shapes of the C_f profiles are similar for different free-stream velocities. Increasing the free-stream velocity causes an overall shift of the profile to lower values of C_f. This is due to the associated increase in Reynolds number that occurs as free-stream velocity is increased (see section 4.2.2). For the case of a trip wire with $d_T = 0.5$ mm and the 80 grit, the location of the peak C_f does not progress upstream with increasing freestream velocity. Interestingly, for the case of a trip wire with $d_T = 0.2$ mm, no local maximum in the C_f profile was resolved and the location of the peak C_f is at the first measurement point downstream of the trip wire (i.e. 5 mm downstream of the trip wire). Taking this point to represent the peak C_f, it is evident from Figure 12 that it also does not move upstream with increasing freestream velocity. It is concluded that wire tripping devices of diameter 0.2 and 0.5 mm, as well as the grit 80 tripping device, are all effective in tripping the boundary layer at the lowest velocity used, i.e. $U_\infty = 40$ m/s, as well as at higher velocities. The data of these devices do not allow the lower limit of the trip Reynolds number to be established.

A limited[2] number of measurements where made with a 0.1 mm wire tripping device at stream-wise stations of 305, 360 and 442 mm for the complete velocity range. Figure 15 shows the data for such a wire compared with data for the 0.2 and 0.5 mm wires as well as data for the un-tripped case. At the lowest freestream velocity the $d_T = 0.1$ mm trip

---

[2]Ideally measurements at all the streamwise stations listed in Table 2 should have been made. However, scheduling of the LSWT did not allow sufficient time for this to occur.
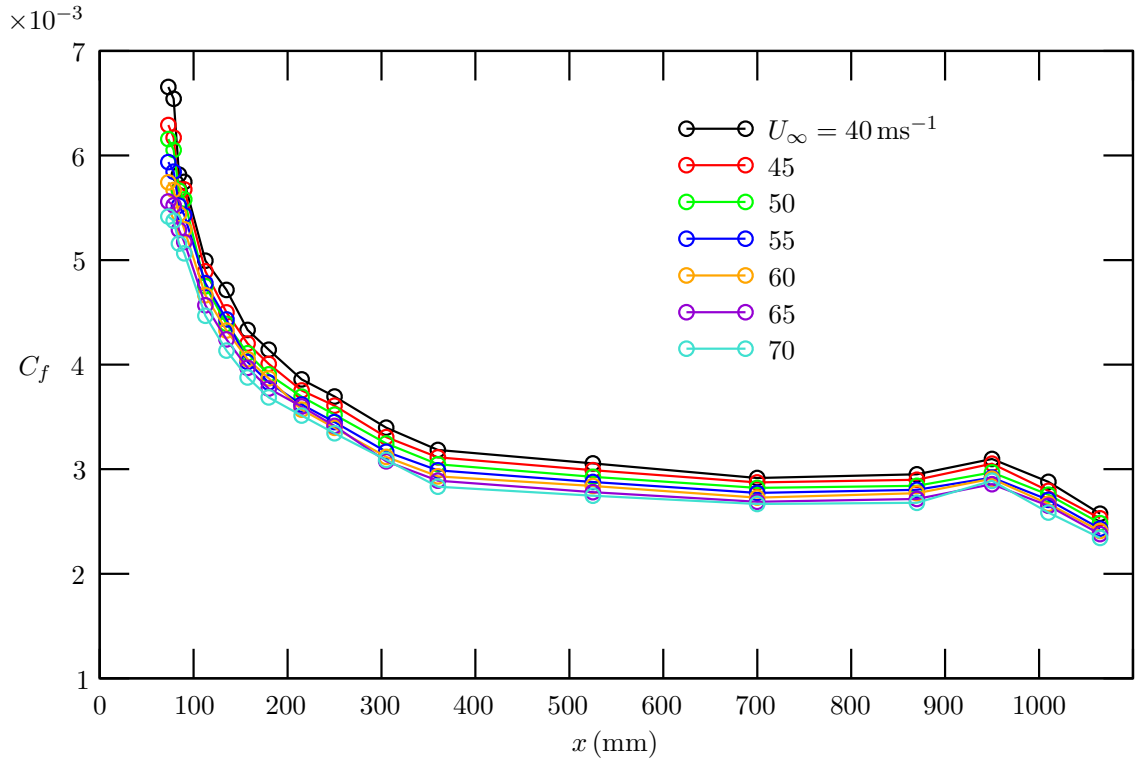
Figure 12: *Skin friction development using a $d_T = 0.2\,mm$ trip wire.*
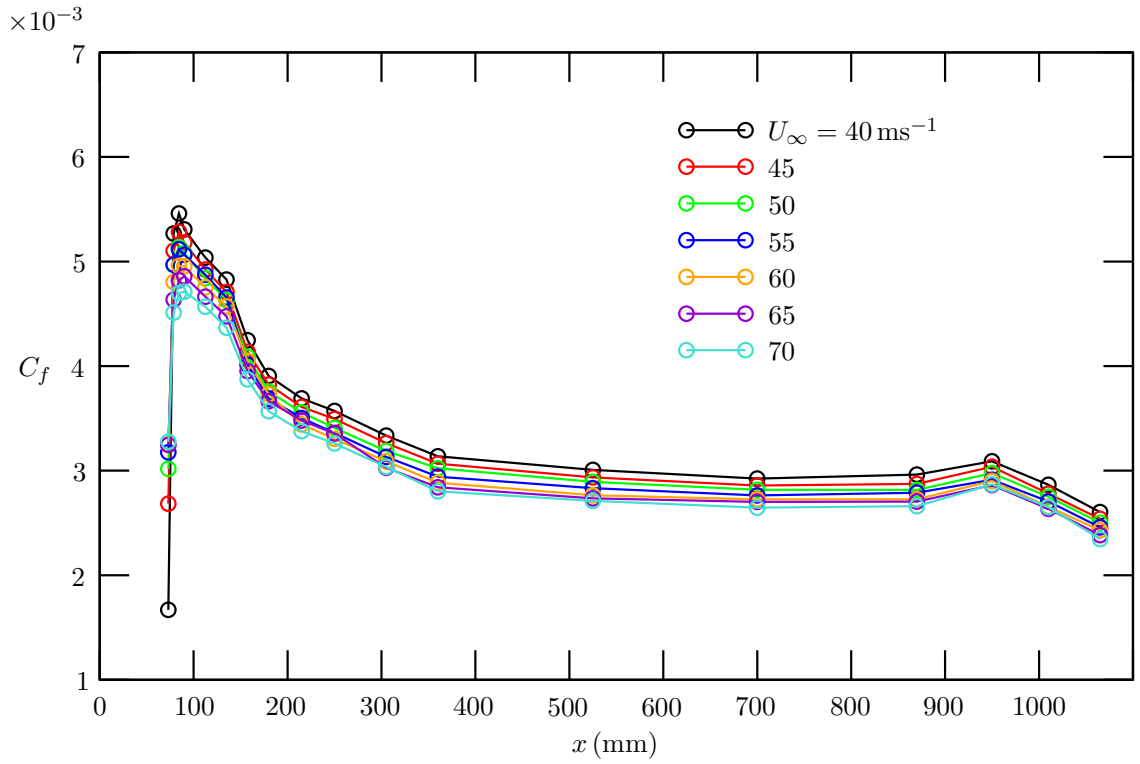
Figure 13: *Skin friction development using a $d_T = 0.5\,mm$ trip wire.*
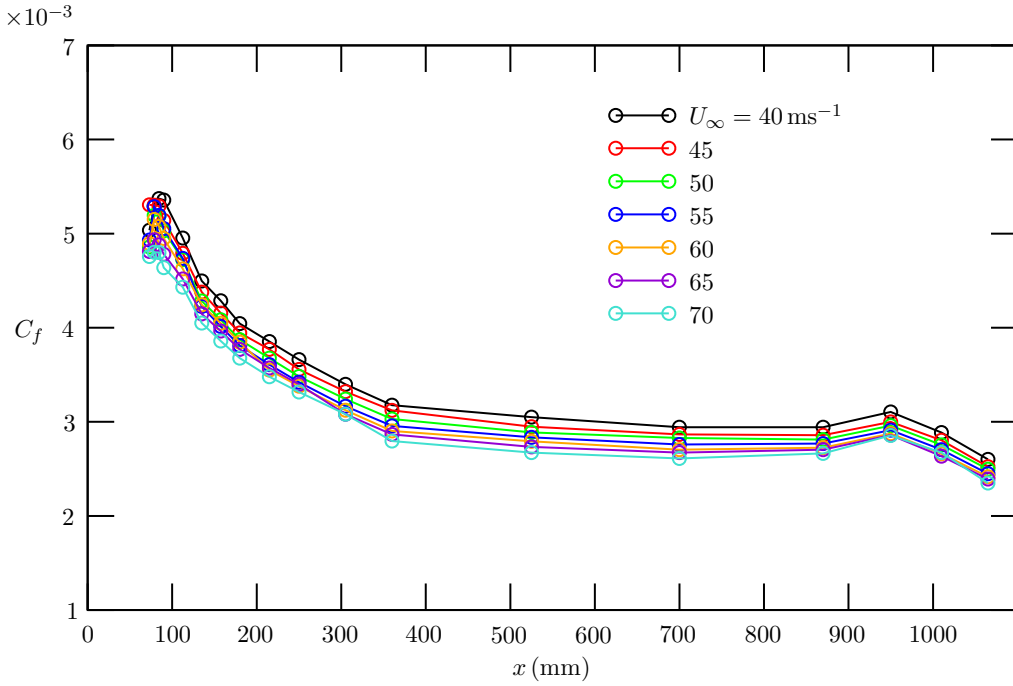
Figure 14: *Skin friction development using 80 grit roughness strip.*

wire did not force transition and the data are similar to those for the un-tripped case (as discussed in Section 4.1, values of C_f for laminar regions are not accurate). The C_f values for the 45 m/s case indicate the boundary layer is in a turbulent state for the $d_T = 0.1$ mm wire. However, the higher values of C_f when compared to the larger diameter trips suggest that transition is not occurring at the trip location but at some point downstream from the trip. In this way the trip is acting to "assist" a natural transition rather than force it. As the free-stream velocity is increased, values of C_f begin to reduce and the results for $U_\infty = 60$ m/s suggest that transition is occurring closer to the tripping device, as for data shown in Figures 12 to 14 for the 0.2 and 0.5 wire tripping devices and the grit 80 device.

The result for the $d_T = 0.1$ mm wire at $U_\infty = 60$ m/s establishes an absolute lower bound on the trip device Reynolds number required to effectively trip the boundary layer. The trip device Reynolds number is defined using the velocity at the edge of the boundary layer, such that

$$Re_{d_T} = \frac{U_1 d_T}{\nu} = \frac{U_\infty d_T \sqrt{1 - C_p}}{\nu}. \tag{13}$$

From the C_p results, given in Section 4.3, it was found that at the location of the trip wire $C_p = -0.07$, also noting the actual freestream velocity was $U_\infty = 62$ m/s for the nominal $U_\infty = 60$ m/s data, yields a trip Reynolds number of $Re_{d_T} = 422$. Given the lack of data collected for the $d_T = 0.1$ mm wire, this value must be treated with caution as it cannot be determined whether the boundary layer remains under-stimulated in the region between the tripping device ($x = 67.5$ mm) and the first measurement station ($x = 305.0$ mm). For the $d_T = 0.2$ mm wire, the lowest value of the trip Reynolds number was $Re_{d_T} = 577$ and, as was shown above, this was effective in causing transition. Therefore it is recommended that $Re_{d_T} = 580$ be taken as the lower limit for the trip device to cause effective transition.

It is important to emphasise that the above finding is only applicable to the current submarine model in the LSWT facility and with the trip device located at $x = 67.5$ mm. The size and type of device to use on the model in other facilities may be different, and could be influenced by many factors, such as the quality of the flow in the tunnel.
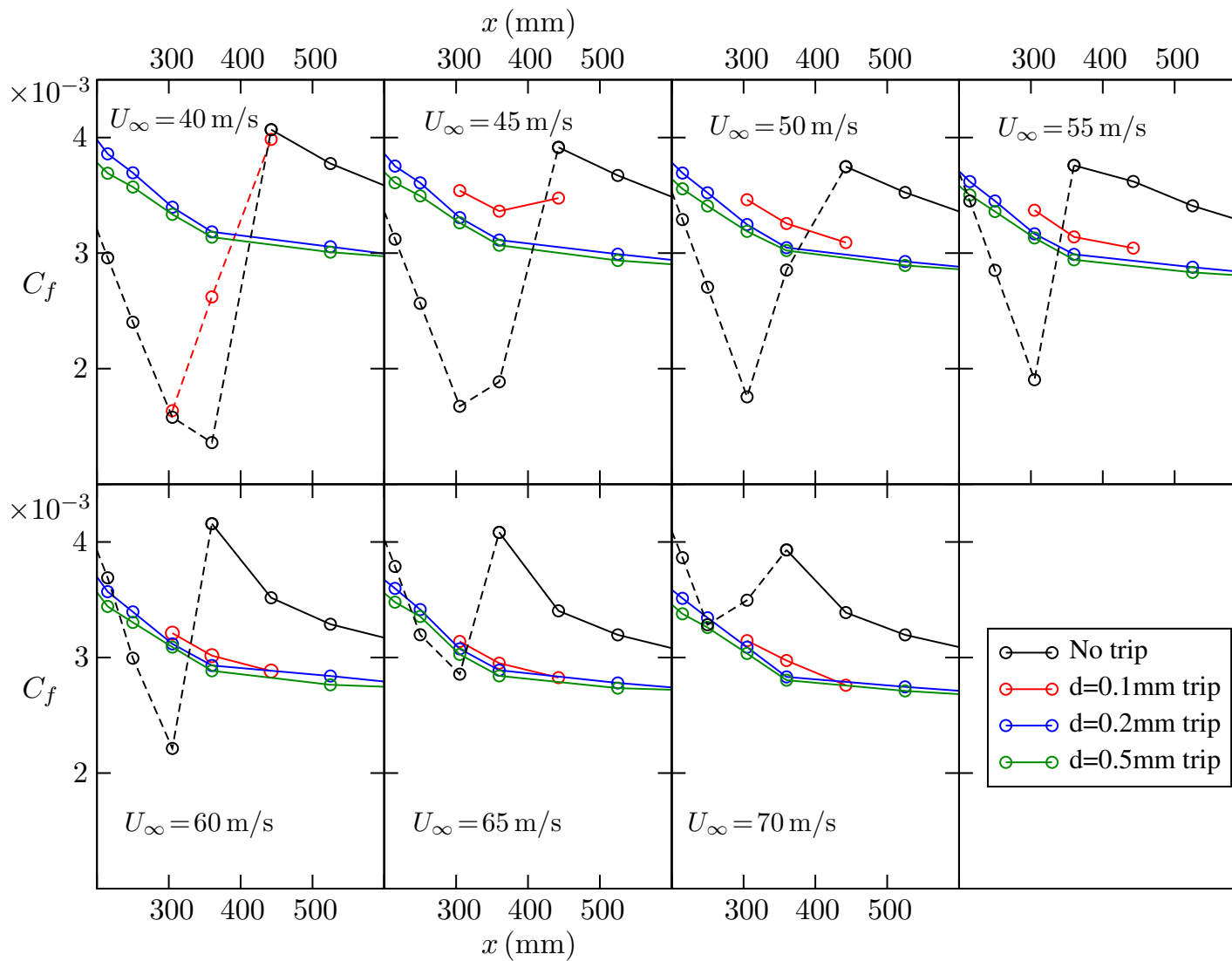
Figure 15: *Comparison of data for the $d_T = 0.1$ mm trip wire and data for the larger trip wires and un-tripped case. The C_f values for laminar regions are not accurate and such data are indicated with dashed lines - see Section 4.1.*

4.2.1   Comparison of the Different Trip Devices

The effect of the different tripping devices on the C_f development is shown in Figure 16, for the case $U = 40_\infty$ m/s. Due to the lack of data, the trip wire $d_T = 0.1$ mm case is not included in these comparisons. As discussed above, the effect of free-stream velocity on the tripped data is a bodily shift of the C_f profiles to lower values as U_∞ is increased. The behaviour of the tripped results for the other free-stream velocities is similar to that shown in Figure 16. However for completeness the equivalent plots for the higher free-stream velocities ($U_\infty = 45 \ldots 70$ m/s) are given in Appendix C.

Based on Figure 16, and the accompanying plots in Appendix C, all three trip devices cause a transition to a turbulent boundary layer. For the stream-wise stations directly downstream of the tripping device, the local effect of the trip device is evident and all three devices read differently in the region directly downstream of the tripping device. This is particularly the case for the $d_T = 0.5$ mm trip wire, which initially under reads significantly, compared with the other two trip devices. The first data point on the curve for the $d_T = 0.5$ mm wire appears to be affected by the wake of the trip device and it is unlikely that the boundary layer profile at this location conforms to a universal wall profile.
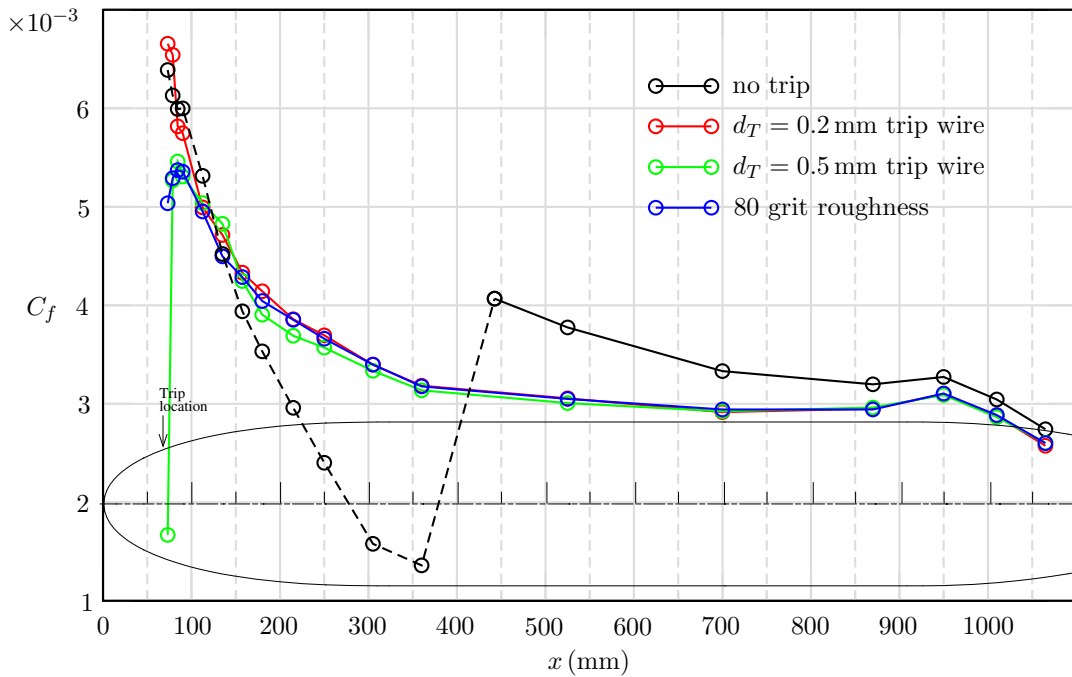
Figure 16: *Comparison of trip devices for $U_\infty = 40$ m/s. For un-tripped data dashed curve indicates a measurement in laminar/transitioning boundary layer. Model profile and trip location also shown.*
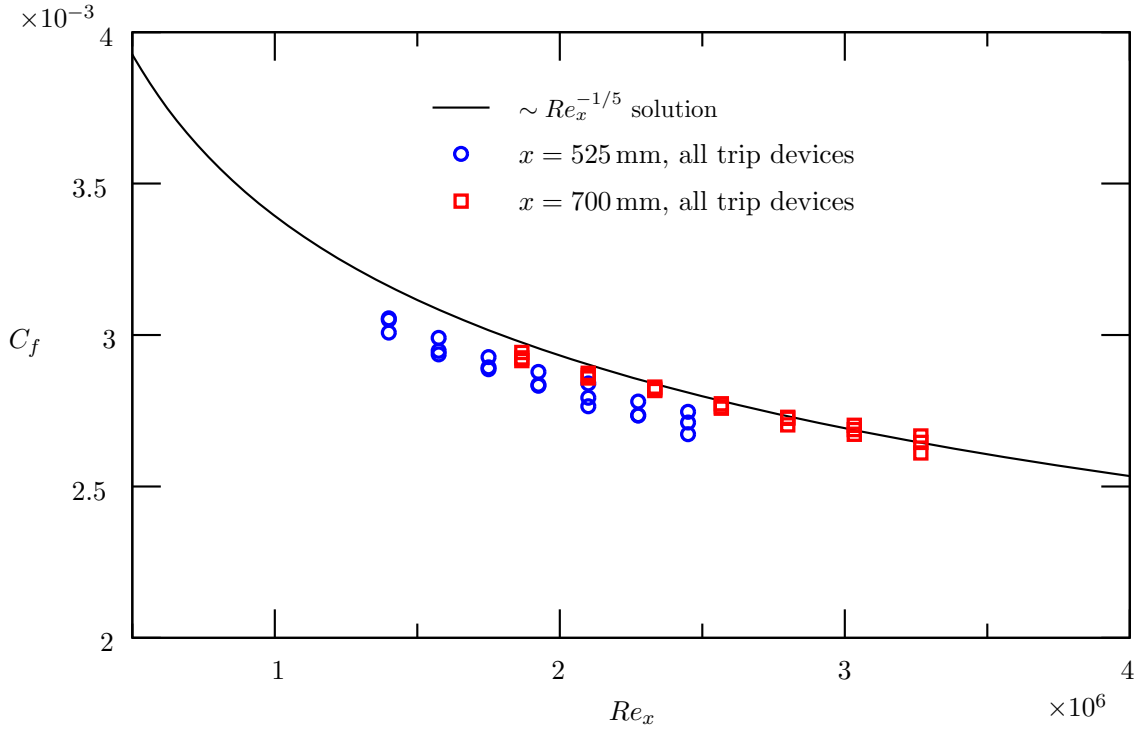
Figure 17: *Comparison of C_f values with flat-plate zero-pressure-gradient solution. Data for stations $x = 525\,mm$ and $x = 700\,mm$ are plotted for all tripping devices.*

4.2.2   Scaling of Skin Friction with Reynolds Number

For a flat plate in a zero pressure gradient the turbulent boundary layer skin friction coefficient approximately scales with $Re_x^{-1/5}$ (Schlichting, 1978), where Re_x is the Reynolds number based on the stream-wise coordinate. The C_f results for the submarine would be expected to be influenced by longitudinal and lateral curvature. However, for the stream-wise coordinates where the pressure gradient is nominally zero, the data are close to the $\sim Re_x^{-1/5}$ solution. Figure 17 shows the $x = 525\,mm$ and $x = 700\,mm$ data for all the tripping devices plotted as a function of Re_x and there is a clear scaling with Re_x.

The $Re_x^{-1/5}$ scaling can be used to achieve reasonable collapse of the skin-friction data across the velocity range of the experiments and this is shown in Figure 18 where the product $C_f Re_x^{1/5}$ is plotted as a function of stream-wise coordinate. This form of scaling is useful in isolating the effects of the tripping device on the skin-friction profiles since it accounts for the Reynolds number variation as freestream velocity is varied. Based on Figure 18 the three devices, trip wires with diameters of $0.2\,mm$, $0.5\,mm$ and 80 grit, all give different readings in the region from the trip to station $x = 360\,mm$. Downstream of station $x = 360\,mm$ the data is considered to have collapsed to within experimental error.

In order to further investigate the local effect of the different tripping devices, Figure 18 is replotted in an enlarged scale for the stations directly downstream of the tripping device, Figure 19. For clarity only data corresponding to $U_\infty \leq 50\,m/s$ is included in Figure 18, and these data corresponds to a trip Reynolds number range $577 \leq Re_{d_T} \leq 1807$.

The $d_T = 0.2\,\text{mm}$ wire and 80 grit tripping devices give different readings directly aft of the tripping device but for stations $x \geq 157.5\,\text{mm}$ the results for these devices collapse, Figure 19. The Reynolds numbers of these two trip devices are close (within 5% at a given velocity) yet they produce different skin friction results for approximately 90 mm downstream of the device and this length corresponds 450 trip heights. This highlights that it is not just the Reynolds number (based on height) of the the device which affects the transition process but also the detailed geometry of the device.

Curves for the $d_T = 0.5\,\text{mm}$ trip wire exhibit a consistent difference from the curves for the other two devices in the region $x < 360\,\text{mm}$, Figure 19. Regions of overshoot and undershoot are evident when compared with the other tripping devices and this behaviour is consistent across the velocity range of the experiments (see Appendix C). The initial under reading, then overshoot/undershoot behaviour of data for the 0.5 mm trip wire suggests it is overstimulating the boundary layer.
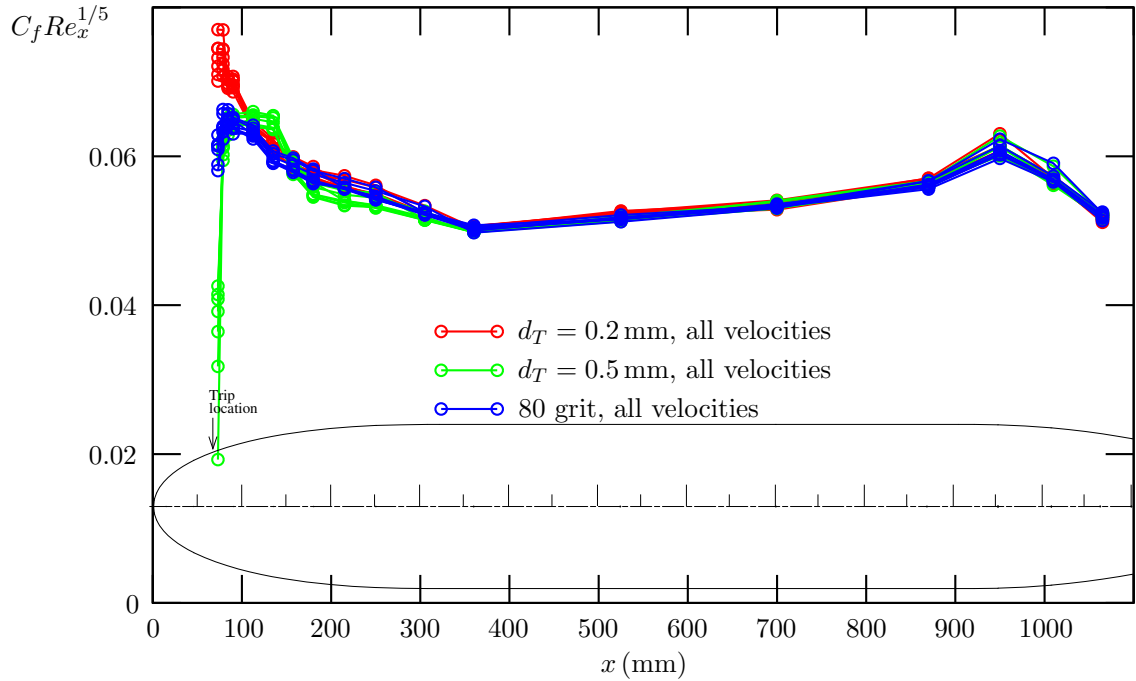
Figure 18: *Scaling skin friction data with Reynolds number. Data for the complete range of velocities and trip devices are included. Model profile and trip location also shown.*

4.2.3   Over-stimulation and the Maximum Trip Reynolds Number

Based on the analysis given in the preceding sections, the trip wire of diameter $d_T = 0.5\,\text{mm}$ is deemed to have overstimulated the transition for all velocities tested. The lowest Reynolds number for this trip device occurs at $U_\infty = 40\,\text{m/s}$, giving a value of $Re_{d_T} = 1443$. However, analysis of the trip wire of diameter $d_T = 0.2\,\text{mm}$ and 80 grit cases indicates that over-stimulation may also be occurring at trip Reynolds numbers lower than this value. Figure 20 shows the skin-friction data for the $d_T = 0.2\,\text{mm}$ and grit cases plotted as the product $C_f Re_x^{1/5}$ versus x, for the complete velocity range, in the region
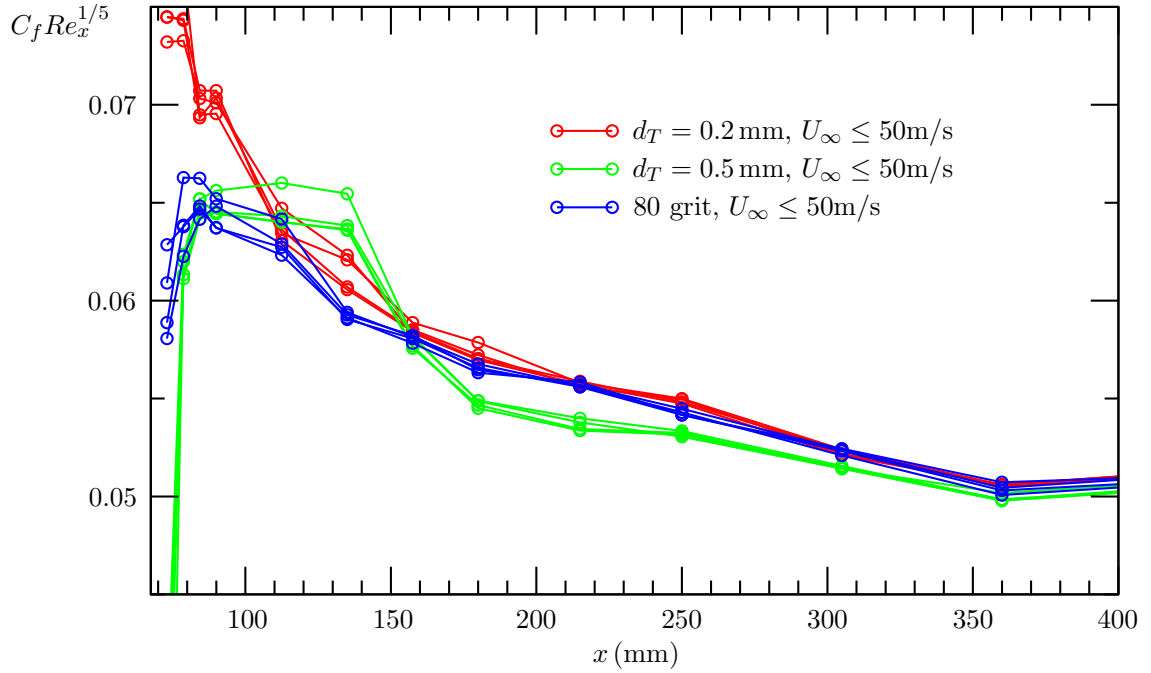
Figure 19: *Scaling skin friction data with Reynolds number. For clarity only data for $U_\infty \leq 50\,m/s$ is included.*

directly aft of the tripping device. For regions upstream of approximately 200 mm the data is scattered and shows no clear trends with U_∞ therefore attention is focused on the data from streamwise station $x = 215\,\text{mm}$ up to station $x = 360\,\text{mm}$. The station $x = 215\,\text{mm}$ corresponds to approximately 700 trip heights downstream of the tripping device while station $x = 360\,\text{mm}$ corresponds to the location where $C_f Re_x^{1/5}$ values collapse across the complete Reynolds number range. This region is shown as a dashed box in Figure 20 and it is clear that all but the two highest freestream velocity cases show good collapse in this region. The trip Reynolds numbers at $U_\infty = 60\,\text{m/s}$ are 865 and 913 for the $d_T = 0.2\,\text{mm}$ wire and 80 grit cases respectively. Based on these numbers it is recommended that the trip Reynolds number not exceed $Re_{d_T} = 900$.

4.3 Pressure Coefficients

For the tripped boundary layer cases, the pressure-coefficient data were found to collapse for the complete range of free-stream velocities. Figure 21 shows pressure coefficients plotted as a function of stream-wise coordinate for the different tripping devices and the un-tripped case for a free-stream velocity of 70 m/s. It is apparent that the C_p data for the case of no tripping device do not collapse indicating the boundary layer growth for this case is different from the data obtained using tripping devices. The lack of collapse is seen more clearly in the zoomed-in plot of Figure 22. This result is consistent with the differences noted in the C_f in Section 4.2.

The C_p results of Figure 21 are almost identical at other free-stream velocities, indicating that any change in boundary layer displacement thickness across the velocity range
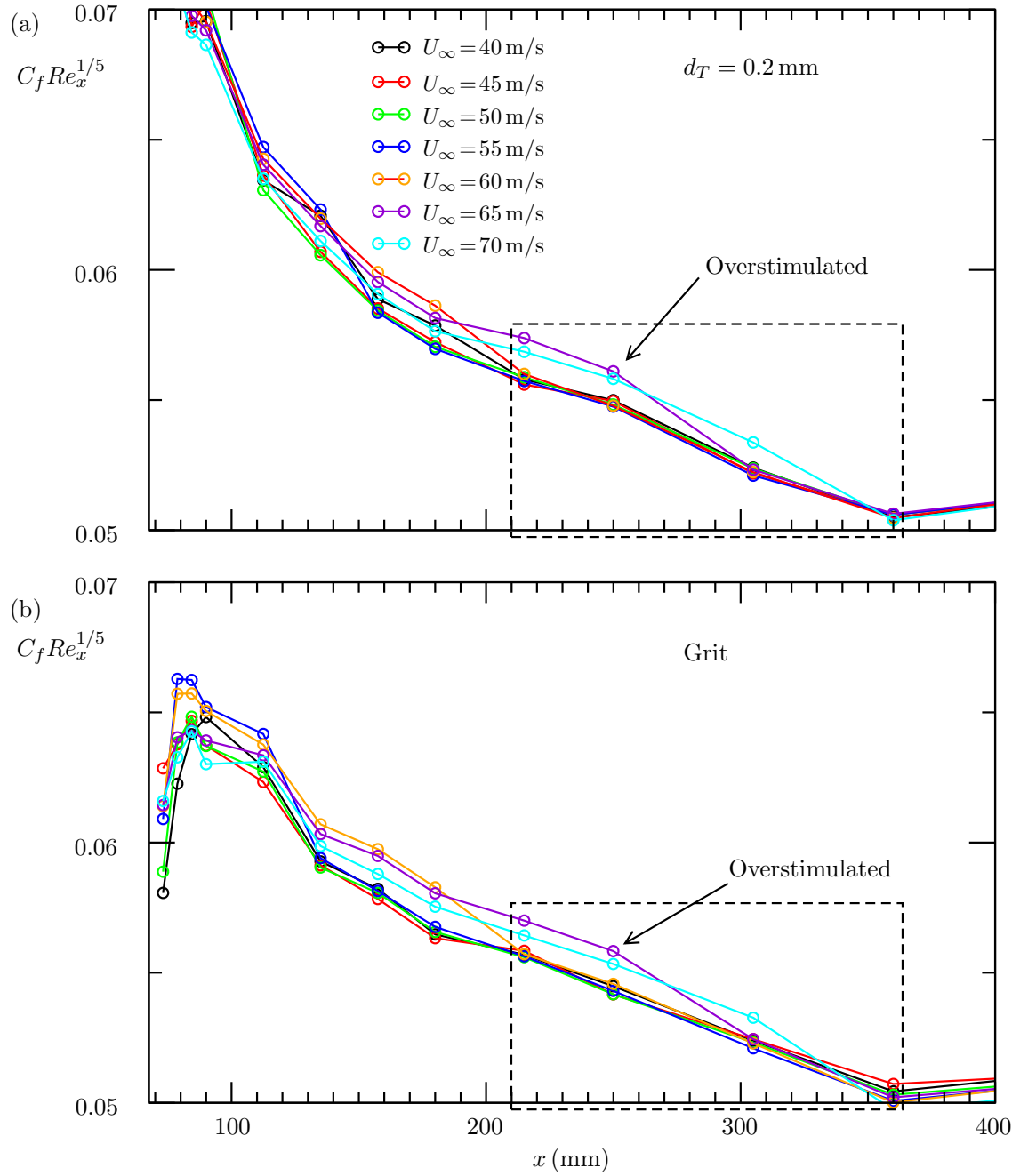
Figure 20: *Comparison of scaled skin-friction for (a) $d_T = 0.2$ mm and (b) 80 grit trip devices. Boxed region indicates region where assessment of data collapse has been made.*
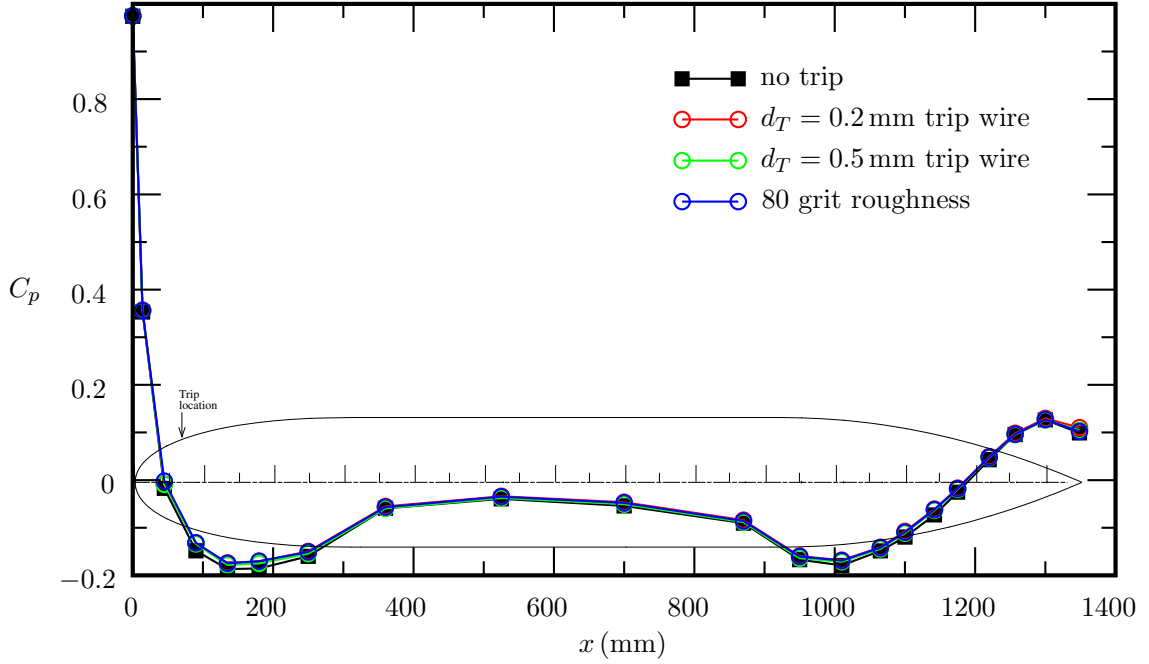
Figure 21: *Pressure coefficient measured at $U_\infty = 70\,m/s$. Model profile and trip location also shown.*

tested has a negligible effect on C_p. The quality of the collapse is illustrated in Figure 23 where the data for the trip wire $d_T = 0.2\,\text{mm}$ case is plotted for the range of free-stream velocities. The C_p data for the other trip devices and for the untripped case are plotted and tabulated in Appendix D.

4.4 Pressure Gradients

As discussed in Section 2, sufficiently strong pressure gradients can modify the law-of-the-wall velocity profile (1), which would affect the accuracy of the Preston-tube calibration curves as given in (4)-(6). For such cases, the non-dimensional pressure gradient parameter p_x^+ enters the analysis (Nickels, 2004) and (1) becomes

$$\frac{U}{U_\tau} = f\left(\frac{U_\tau y}{\nu}, p_x^+\right). \tag{14}$$

The parameter p_x^+ would then be present in the forms of (4)-(6) and would need to be calibrated. However, provided p_x^+ remains within the experimentally-determined limits of the Patel (1965) calibration, the effect on the Preston-tube calibration is small. Figure 24 shows the pressure gradient parameter for the $d_T = 0.2\,\text{mm}$ trip wire case and it is evident that the data is within the 3% error band of $-0.005 < p_x^+ < 0.01$, as specified by (9a) and (10a).
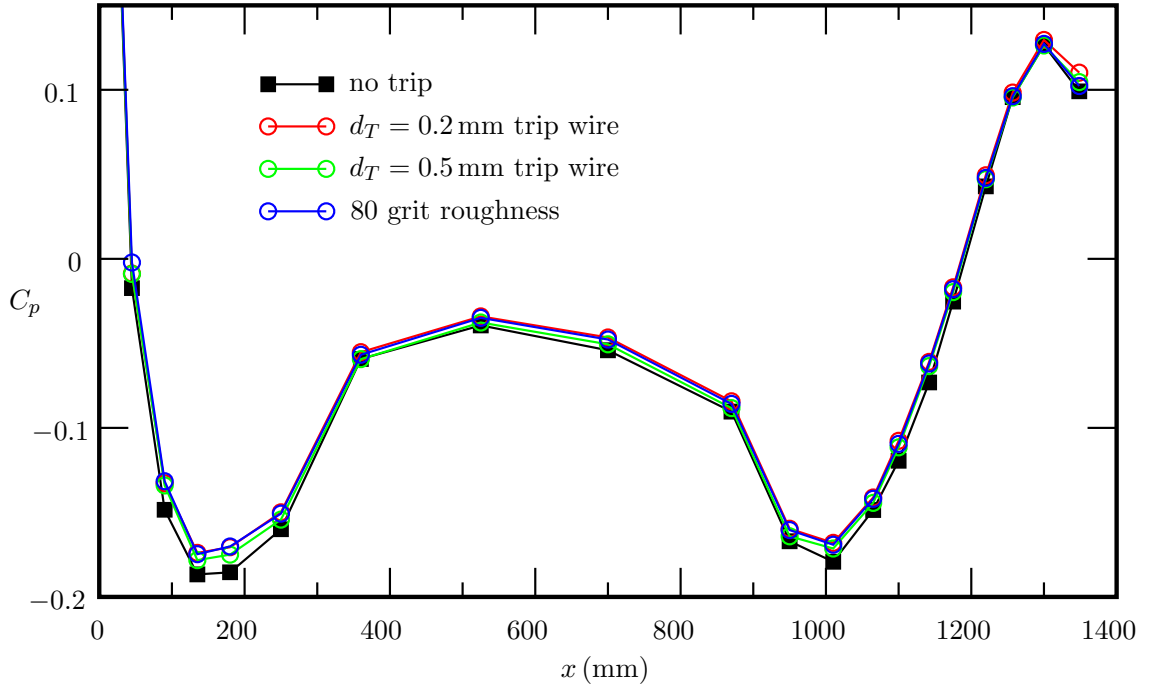
Figure 22: *Re-plot of Figure 21, with an expanded C_p axis, showing more clearly the difference between the tripped and un-tripped data.*
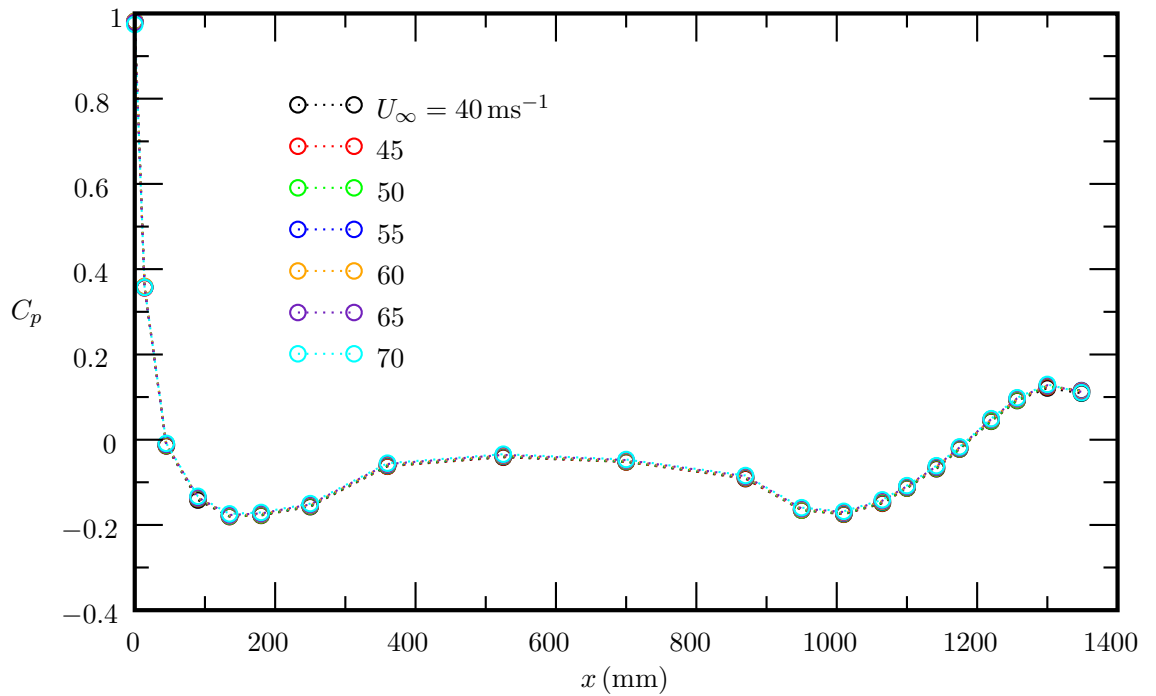
Figure 23: *Pressure coefficient across the range of free-stream velocities for the trip wire $d_T = 0.2\,mm$ case.*
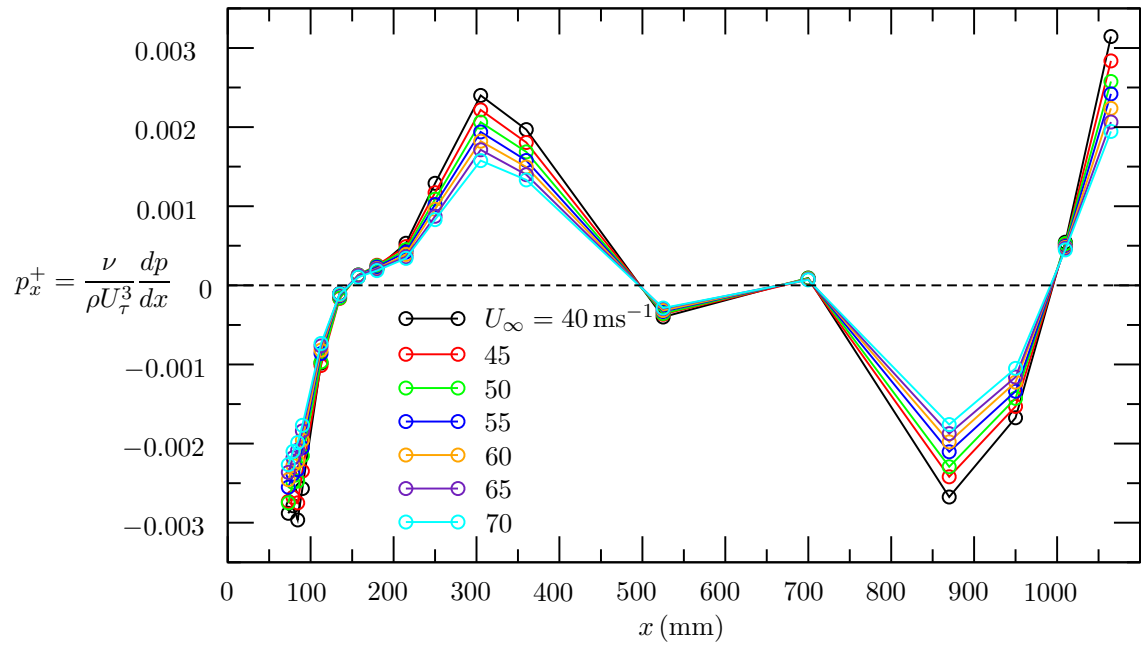
Figure 24: *Non-dimensional pressure gradient across the range of free-stream velocities for the trip wire $d_T = 0.2\,mm$ case.*

5   Comparison with CFD Predictions

In parallel to the experimental program, CFD methods are being developed for submarine geometries. The commercial CFD package *Fluent* has been benchmarked against existing experimental and numerical results (for the "DARPA SUBOFF" model) to determine appropriate meshes and turbulence models to use. Details of the CFD work are given in Snowden & Widjaja (2011). Based on the findings of Snowden & Widjaja further CFD predictions have recently been performed for the Joubert submarine model (Snowden, private communication).

The CFD predictions, applied to the Joubert submarine model (including the support pylon and actuator arm) are shown in Figures 25 and 26. The CFD C_p results agree well with the current experimental results, Figure 25. However the CFD C_f results are greater than the C_f data using tripping devices (e.g. data for $d_T = 0.2\,\text{mm}$, Figure 26). The CFD model imposes a turbulent-boundary-layer solution from the nose of the model ($x = 0$) whereas the experimental results correspond to using tripping devices at $x = 67.5\,\text{mm}$. The current results demonstrate the sensitivity of the C_f evolution to the point of transition (compare the data for no trip device data with those using tripping devices) and this may explain the difference between CFD and experimental data. However further work is required to make firm conclusions regarding the differences in Figure 26. Perhaps CFD could be applied to the case in which the boundary layer is laminar up to the tripping device and turbulent thereafter.
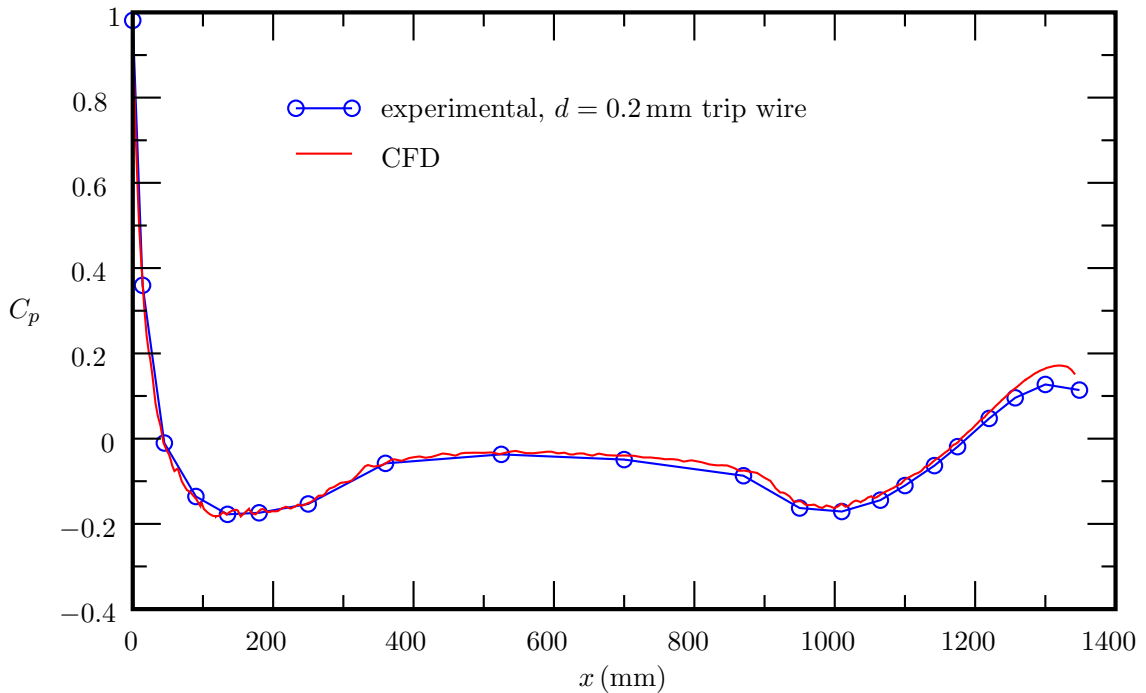
Figure 25: *Comparison of experimental C_p measurements with CFD results for the Joubert submarine model. Experimental data for $d_T = 0.2\,mm$ wire for $U_\infty = 60\,m/s$.*
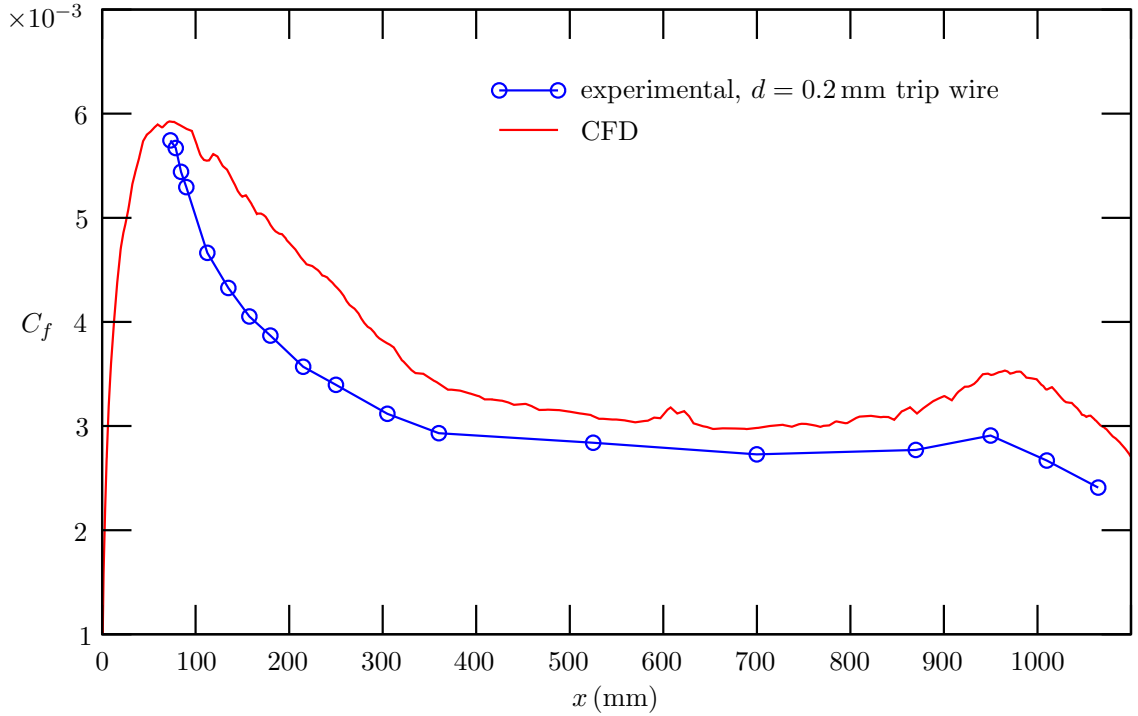
Figure 26: *Comparison of Preston tube skin-friction measurements with CFD results for the Joubert submarine model. Experimental data for $d_T = 0.2$ mm wire with $U_\infty = 60$ m/s.*

6   Conclusions

Use of the Preston-tube technique to measure turbulent skin friction coefficients along the upper surface of a generic submarine model in the LSWT was shown to be valid. Turbulent skin-friction coefficients were measured for free-stream velocities varying from 40 m/s to 70 m/s for the case of no tripping device, for wires of diameter 0.1, 0.2 and 0.5 mm, and for silicon carbide grit of size 80. The tripping devices were located 67.5 mm downstream of the nose of the model, which corresponds to 5 % of its length.

The wire of diameter 0.2 mm and the grit of size 80 where found to correctly stimulate transition, for freestream velocities varying from 40 m/s to 60 m/s. For freestream velocities higher than 60 m/s both these devices appeared to be slightly overstimulating the boundary layer transition process. The average height ($h = 0.21$ mm) of the grit elements was only slightly more than the wire of diameter 0.2 mm. However, differences in the skin friction values directly aft of these tripping devices were evident for approximately 450 trip heights downstream of the respective devices. From a model testing point of view these differences are considered to be negligible and, of these two devices, the wire is the preferred option since it was observed that grit may erode during a testing program.

The wire of diameter 0.5 mm was found to overstimulate the boundary layer transition process for the complete velocity range of the experiments. For the wire of diameter 0.5 mm, the effect of the over-stimulation was evident in the skin friction measurements for approximately 600 trip diameters downstream of the trip device. Beyond this location, the skin friction results for the wires of diameters 0.2 and 0.5 mm, and for the grit were

found to agree with each other.

Only a limited range of streamwise data were collected for the trip wire of diameter 0.1 mm. However there were sufficient data to show that for freestream velocities less than 60 m/s that this device was under-stimulating the boundary layer transition. The limited data for this case meant it was not possible to accurately determine the lowest velocity for which this device correctly stimulated the transition.

Based on the current results, it is recommend that trip device be sized such that the Reynolds number of the trip device lies within the range $580 \leq Re_{d_T} \leq 900$. This ensures that the boundary layer transition is correctly stimulated. Under-stimulation of the boundary layer will generally have a more significant effect on the resulting skin-friction values when compared to the case of over-stimulation, where the effects are more subtle. Therefore the upper bound of the above range can be relaxed slightly when carrying out tests over a range of freestream velocities and using a model with a fixed trip size.

The above limits for Re_{d_T} only apply in the LSWT for the Joubert model with a tripping device located at 5% of the model length. The findings cannot be directly applied to other models tested in different tunnels due to possible differences in roughness of a model, pressure gradient about the nose of the model, free-stream turbulence level, noise generated by the tunnel wall boundary layers, vibration of a model, and flow irregularities in the free-stream.

It was found that reasonable collapse of the skin-friction data across the velocity range of the experiments could be achieved if the skin friction data is multiplied by the local Reynolds number to the power 1/5, i.e. the product $C_f Re^{1/5}$ is a function of streamwise coordinate alone.

Whilst the Preston tube cannot be used to quantify the laminar skin friction, it was found to provide a simple means of estimating the point of natural transition for the cases without a tripping device. Without a tripping device, natural transition of the boundary layer ranged between approximately $x = 340\,\text{mm}$ (at $U_\infty = 40\,\text{m/s}$) to $260\,\text{mm}$ (at $U_\infty = 70\,\text{m/s}$) which corresponds to 25% and 19% of the model length respectively and Reynolds numbers of 0.91×10^6 and 1.22×10^6 respectively.

Skin-friction coefficients measured on the submarine model in the LSWT were compared with CFD predictions for a limited number of tests. Differences occurred between experimental and predicted data, possibly due to differences in the extent of turbulent flow over the model for the two cases. For the experiments, the flow was found to be turbulent downstream of the tripping devices, whereas for the CFD predictions, a turbulent flow was imposed over the entire length of the model.

Pressure coefficients measured along the top surface of the submarine model were found to show good agreement for the cases where a tripping device was used. The measured pressure coefficients showed good agreement with CFD predictions for the limited data compared.

Further work is required to quantify the boundary layer profile on the scale model, which would provide an improved means of assessing the effectiveness of the trip devices used. In addition, the use of smaller trip devices could introduce errors into the measurements due to the difficulty in locating and attaching them on the surface of the model. Alternative tripping devices, such as cylindrical pins, need to be considered.

7   Acknowledgements

References

Braslow, A. L. & Knox, E. (1958). Simplified method for determination of critical height of distributed roughness particles for boundary-layer transition at Mach numbers from 0 to 5. Technical Note TN-4363, NASA.

Coles, D. E. (1956). The law of the wake in the turbulent boundary layer. *J. Fluid Mech.*, 1, 191–226.

Coles, D. E. (1962). The turbulent boundary layer in a compressible fluid. Technical Report Rep. R-403-PR, The Rand Corporation. Appendix A: A manual of experimental boundary-layer practice for low-speed flow.

Erm, L. P. (2003). Calibration of the flow in the extended test section of the low-speed wind tunnel at DSTO. Tech. Rep. DSTO-TR-1384, Defence Science and Technology Organisation, Melbourne, Australia.

Erm, L. P. & Joubert, P. N. (1991). Low-Reynolds-number turbulent boundary layers. *J. Fluid Mech.*, 230, 1–44.

Fage, A. & Preston, J. H. (1941). On transition from laminar to turbulent flow in the boundary layer. *Proceedings of the Royal Society of London. Series A. Mathematical and Physical Sciences*, 178(973), 201–227.

Fernholz, H. H., Janke, G., Schober, M., Wagner, P. M., & Warnack, D. (1996). New developments and applications of skin-friction measuring techniques. *Meas. Sci. Technol*, 7, 1396–1409.

Gibbings, J. C. (1959). Boundary layer transistion: Prediction, application to drag reduction. Technical Report CP-462, Aero Research Council.

Gregory, P. (2006). *Flow over a body of revolution in a steady turn.* Ph.D. thesis, Department of Mechanical and Manufacturing Engineering, The University of Melbourne.

Groves, N. C., Huang, T. T., & Chang, M. S. (1989). Geometric characteristics of darpa suboff models models (dtrc model nos. 5470 and 5471). Technical Report DTRC/SHD-1298-01., David Taylor Research Center, Bethesda, MD.

Hosder, S. (2001). *Unsteady Skin-Friction measurements on a Maneuvering Darpa2 Suboff Model.* Master's thesis, Aerospace Engineering, Virginia Polytechnic Institute and State University.

Jimenez, J. (2004). Turbulent flows over rough walls. *Ann. Rev. Fluid Mech.*, 36, 173–196.

Jimenez, J. M., Hultmark, M., & Smits, A. J. (2010a). The intermediate wake of a body of revolution at high Reynolds numbers. *J. Fluid Mech.*, 659, 516–539.

Jimenez, J. M., Reynolds, R. T., & Smits, A. J. (2010b). The effects of fins on the intermediate wake of a submarine model. *J. Fluids Eng.*, 132.

Joubert, P. N. (2004). Some aspects of submarine design part 1. hydrodynamics. DSTO-TR 1622, DSTO.

Joubert, P. N. (2006). Some aspects of submarine design part 2. shape of a submarine 2026. DSTO-TR 1920, DSTO.

Loid, H. & Bystrom, L. (1983). Hydrodynamic aspects of the design of the forward and aft bodies of the submarine. In *RINA International Symposium on Naval Submarines*. Paper No. 19.

Nickels, T. B. (2004). Inner scaling for wall-bounded flows subject to large pressure gradients. *J. Fluid Mech.*, 521, 217–239.

Patel, V. (1965). Calibration of the Preston tube and limitations on its use in pressure gradients. *J. Fluid Mech.*, 23, 185–205.

Preston, J. (1954). The determination of turbulent skin friction by means of Pitot tubes. *J. Royal Aero. Soc.*, 58, 109–121.

Reed, H. & Saric, W. (2008). Transition mechanisms for transport aircraft. In *38th AIAA Fluid Dynamics Conference and Exhibit*.

Schlatter, P. & Henningson, D. S., editors (2009). *Proceedings of the Seventh IUTAM Symposium on Laminar-Turbulent Transition*. IUTAM, Stockholm, Sweden.

Schlichting, H. (1978). *Boundary Layer Theory*. McGraw-Hill. Seventh Edition.

Snowden, A. D. & Widjaja, R. (2011). CFD modelling of the DARPA SUBOFF submarine model in bare hull configuration. Tech. Rep. DSTO-TR-2551, Defence Science and Technology Organisation, Melbourne, Australia.

Tani, I., Hama, R., & Mituisi, S. (1940). On the permissible roughness in the laminar boundary layer. Technical Report 199, Aero. Res. Inst. Tokyo, Imp. Uni. Also published as NASA-TM-89802.

Tani, I. & Sato, H. (1956). Boundary-layer transition by roughness element. *Journ. Phys. Soc., Japan*, 12(12), 1284.

Watt, G. D., Nguyen, V. D., Cooper, K. R., & Tanguay, B. (1993). Wind tunnel investigations of submarine hydrodynamics. *Canadian Aeronautics and Space Journal*, 39(3), 119–126.

Wetzel, T. G. & Simpson, R. L. (1996). Unsteady flow over a 6:1 prolate spheroid. Technical Report VPI-AOE-232, Advanced Research Projects Agency, through the Office of Naval Research, Applied Hydrodynamics, Arlington, VA, USA.

White, F. M. (1974). *Viscous Fluid Flow.* McGraw-Hill, New York.

Whitfield, C. C. (1999). *Steady and unsteady force and moment data on a DARPA2 submarine.* Master's thesis, Aerospace Engineering, Virginia Polytechnic Institute and State University.

Zagarola, M., Williams, D., & Smits, A. (2001). Calibration of the Preston probe for high Reynolds number flows. *Measurement Science and Technology*, 12(4), 495–501.

Appendix A   Summary of Tripping Devices Used in Previous Experiments

Table A1: *Summary of tripping devices used in previous experiments. Here d is the wire or pin diameter, h is the pin height and s is the pin spacing.*

Researchers	Model	Air or Water	L (mm)	D (mm)	Trip Device (units mm)	Trip location (mm)	Trip location (% of L)	U_∞ (m/s)	Re ($\times 10^6$)
Groves et al. (1989)	SUBOFF	Both	4356	508	Wire: $d = 0.635$	215.9	4.96	not given	not given
Groves et al. (1989)	SUBOFF	Air	4356	508	Wire: $d = 0.635$	215.9	4.96	not given	not given
Watt et al. (1993)	Submarine	Air	6000		Three dimensional		3		23
Wetzel & Simpson (1996)	prolate spheroid	Air	1370	229	not given	274	20	45	4.2
Whitfield (1999)	DARPA2 submarine	Air	2236	267	Cylindrical pins: $h = 0.762$ $d = 1.27$	304.8		30.5 & 42.7	4.2 & 6.1
Hosder (2001)	DARPA2 SUBOFF	Air	2240		Cylindrical pins: $h = 0.76$, $d = 1.28$ $s = 2.5$		10	42.7	5.5
Gregory (2006)	Bodies of revolution straight and bent	Air	2580	260	Cylindrical pins: $h = 0.203$, $d = 0.305$ $s = 1.27$		5	15	2.58
Jimenez et al.(2010a)	SUBOFF	Air	870	102	Wire: $d = 0.51$	76.5	8.79		1.1 to 67
Jimenez et al.(2010b)	SUBOFF	Air	870	101.6	Wire: $d = 1.0$	25.4	2.92		0.49 & 1.8
Unknown	prolate spheroid	Air	1370	229	Cylindrical pins: $h = 0.7$, $d = 1.2$, $s = 2.5$		20	50.7 to 55.2	4.2

Appendix B   Preston Tube Data Processing

A C-language computer program, named `PSI_skin-friction.c`, was written to convert the Preston-tube pressure measurements to skin-friction coefficients. The program takes as input an experimental data file created by the ImPressOne data acquisition software, a file containing the C_p distributions (for the given trip device), a file containing the fluid properties logged during the experiment (for the given trip device) and the location of the Preston tube. The output of the program `PSI_skin-friction.c` contains the skin friction results at a given x coordinate for the range of freestream velocities tested, Figure B1 summarises the input and output files. Note, for each trip device there is a series of ImPressOne data files where each file corresponds to a unique location of the Preston tube. The ImPressOne data file contains the averaged samples for all pressure ports, in blocks of data corresponding to the different freestream velocities.
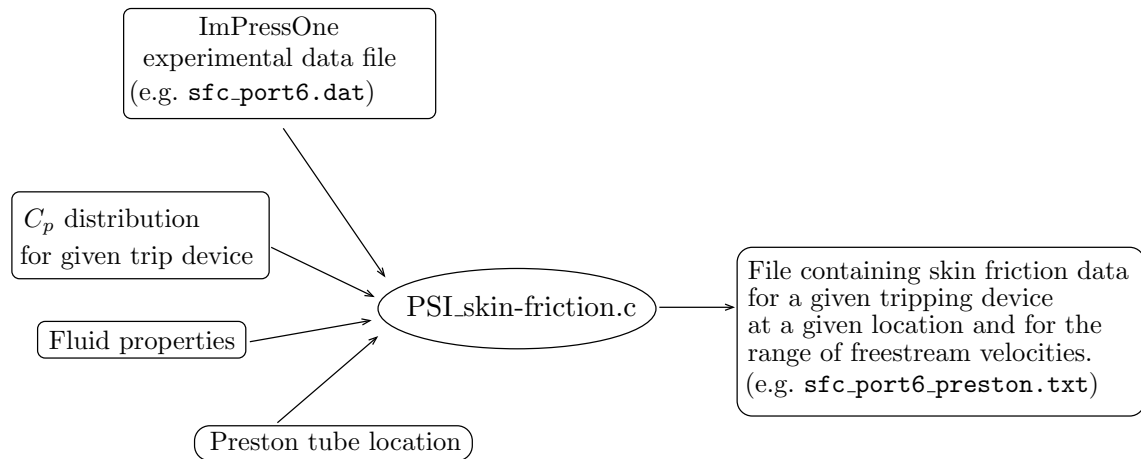
Figure B1: *Input and output of program* `PSI_skin-friction.c`.

Once all experimental data files have been processed, the results can be collated into a file containing the skin friction coefficients as a function of x, for a given trip device and for a given freestream velocity using the C-language computer program, named `merge_data.c`.

The source code for `PSI_skin-friction.c` and `merge_data.c` are contained in the following attachments, which can be accessed by right-clicking on the icon.

<div align="center">

`PSI_skin-friction.c` 📎   `merge_data.c` 📎

</div>

Example input files for the program `PSI_skin-friction.c` are provided in the following attachments. The data files correspond to the experiment where a 0.5 mm trip wire was used.

<div align="center">

`sfc_port6.dat` 📎   `Cp_trip-wire05.txt` 📎   `fluid-properties.txt` 📎

</div>

Appendix C   Skin Friction Coefficients
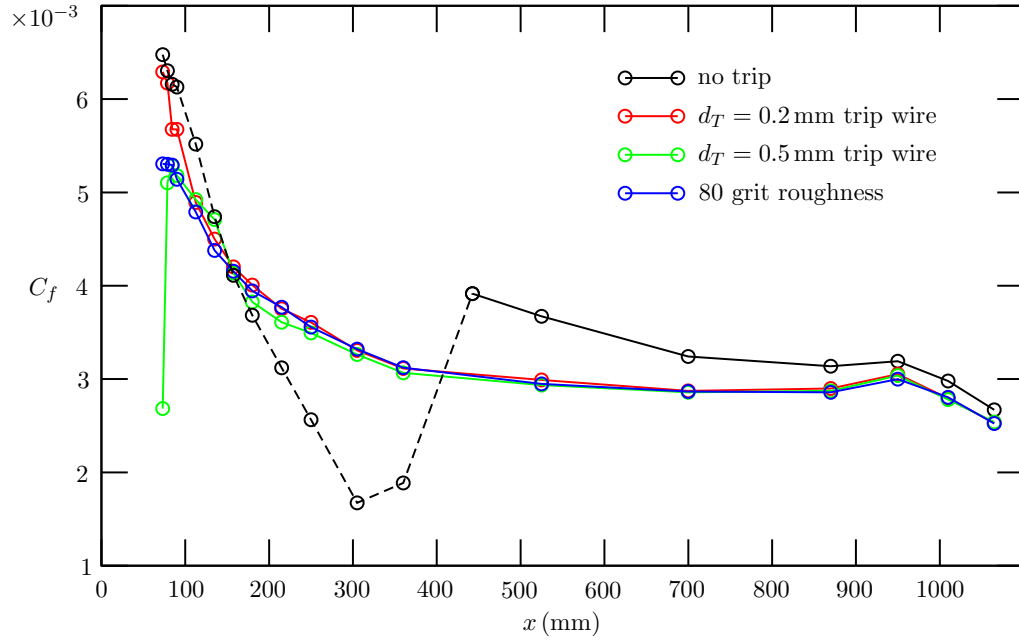
Figure C1: *Comparison of trip devices for $U_\infty = 45\,m/s$. Dashed lines indicate data were obtained in a laminar or transitioning boundary layer and in these regions the Preston tube method breaks down.*
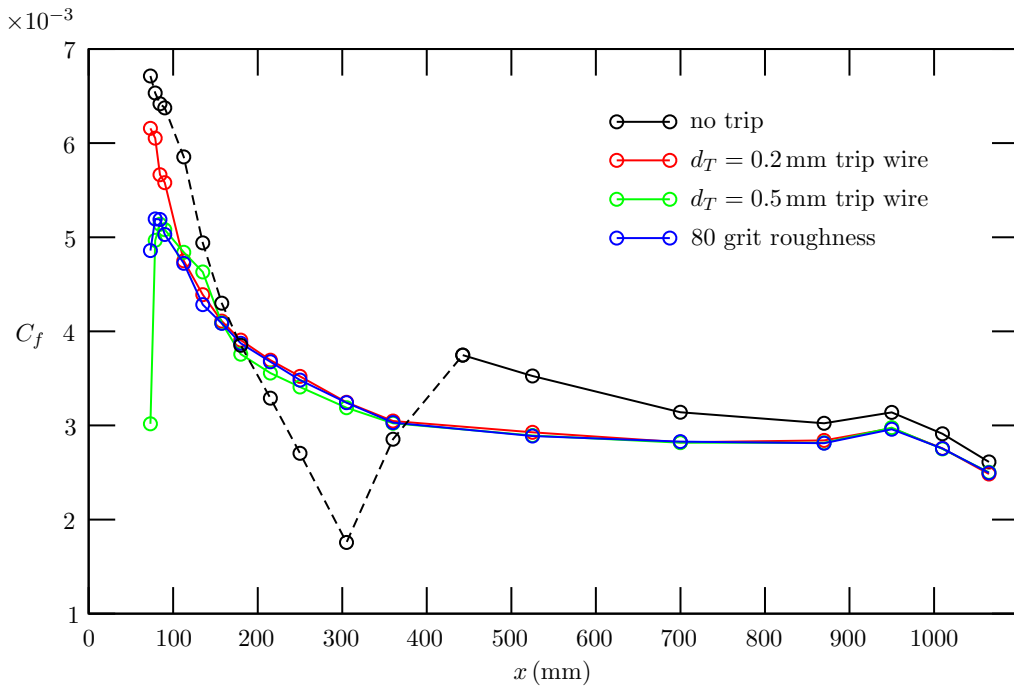
Figure C2: *Comparison of trip devices for $U_\infty = 50\,m/s$. Dashed lines indicate data were obtained in a laminar or transitioning boundary layer and in these regions the Preston tube method breaks down.*
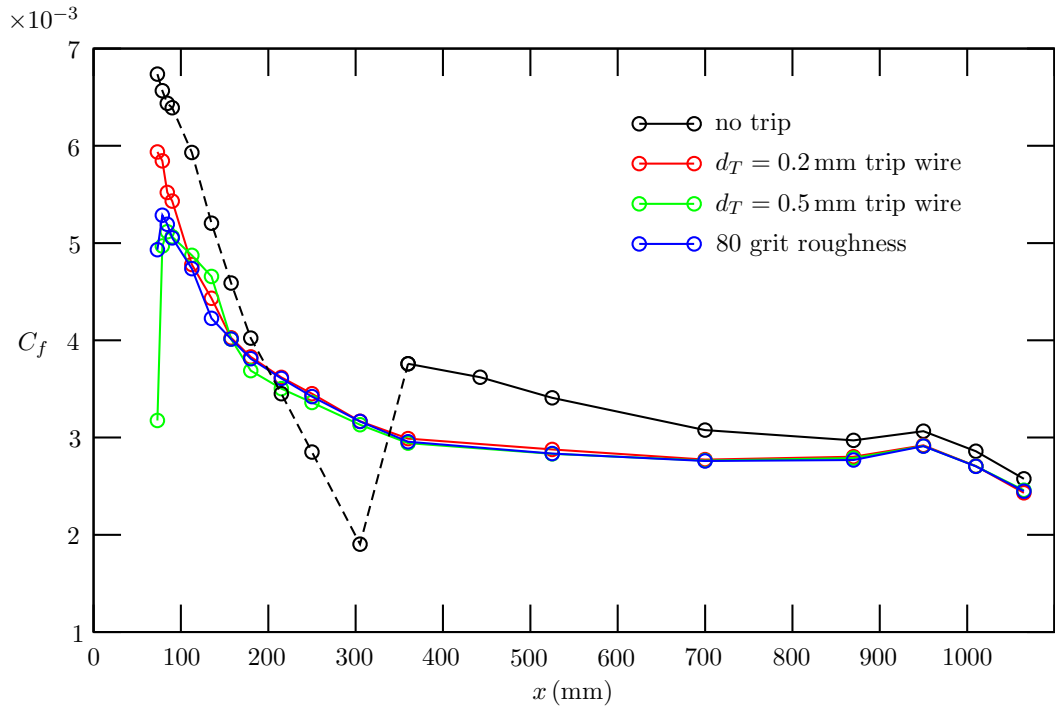
Figure C3: *Comparison of trip devices for $U_\infty = 55\,m/s$. Dashed lines indicate data were obtained in a laminar or transitioning boundary layer and in these regions the Preston tube method breaks down.*
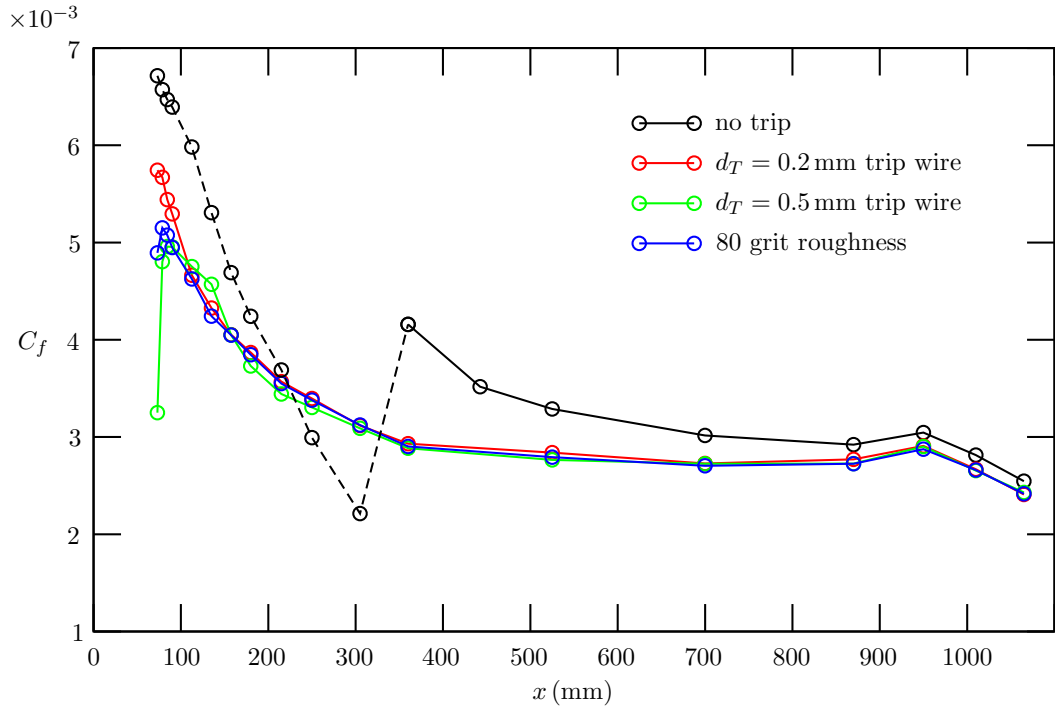
Figure C4: *Comparison of trip devices for $U_\infty = 60\,m/s$. Dashed lines indicate data were obtained in a laminar or transitioning boundary layer and in these regions the Preston tube method breaks down.*
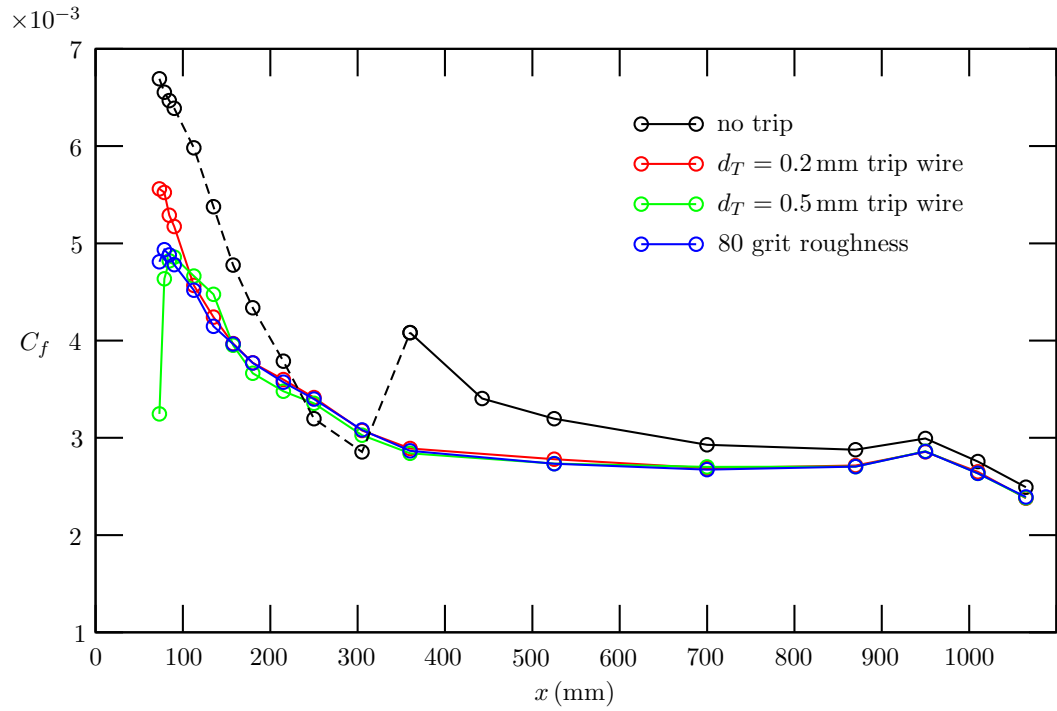
Figure C5: *Comparison of trip devices for $U_\infty = 65\,m/s$. Dashed lines indicate data were obtained in a laminar or transitioning boundary layer and in these regions the Preston tube method breaks down.*
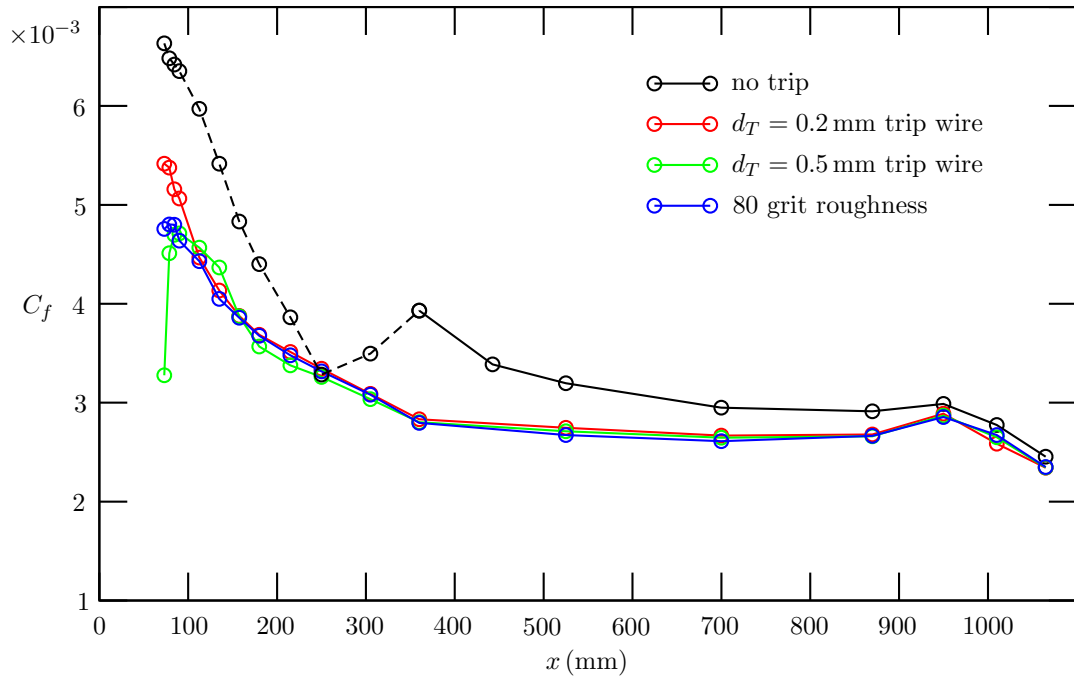
Figure C6: *Comparison of trip devices for $U_\infty = 70\,m/s$. For un-tripped data dashed curve indicates a measurement in laminar/transitioning boundary layer.*

Table C1: C_f data for case of no trip device. Bracketed values indicated a laminar boundary layer and values are provided for qualitative assessment only.

x (mm)	$U_\infty = 40\,\mathrm{m/s}$		45		50		55		60		65		70	
	Re_x	C_f	Re_x	C_f	Re_x	C_f	Re_x	C_f	Re_x	C_f	Re_x	C_f	Re_x	C_f
73.07	0.207	(6.388)	0.234	(6.476)	0.262	(6.714)	0.287	(6.738)	0.313	(6.715)	0.340	(6.693)	0.369	(6.634)
78.70	0.225	(6.131)	0.254	(6.304)	0.283	(6.533)	0.313	(6.567)	0.341	(6.572)	0.371	(6.554)	0.403	(6.482)
84.34	0.244	(5.993)	0.275	(6.158)	0.305	(6.419)	0.337	(6.437)	0.369	(6.471)	0.400	(6.468)	0.433	(6.418)
89.97	0.263	(6.000)	0.296	(6.129)	0.328	(6.375)	0.362	(6.392)	0.395	(6.393)	0.431	(6.389)	0.466	(6.352)
112.47	0.332	(5.314)	0.375	(5.517)	0.415	(5.853)	0.459	(5.931)	0.501	(5.982)	0.545	(5.982)	0.591	(5.970)
134.97	0.401	(4.520)	0.449	(4.740)	0.500	(4.940)	0.552	(5.204)	0.605	(5.308)	0.656	(5.377)	0.707	(5.416)
157.47	0.467	(3.939)	0.527	(4.112)	0.586	(4.300)	0.645	(4.589)	0.704	(4.691)	0.765	(4.776)	0.831	(4.832)
179.97	0.535	(3.532)	0.601	(3.684)	0.667	(3.852)	0.737	(4.023)	0.806	(4.242)	0.868	(4.338)	0.948	(4.401)
214.97	0.637	(2.959)	0.715	(3.121)	0.795	(3.290)	0.877	(3.451)	0.958	(3.690)	1.041	(3.788)	1.128	(3.864)
249.97	0.733	(2.402)	0.828	(2.565)	0.917	(2.704)	1.012	(2.851)	1.108	(2.994)	1.203	(3.197)	1.303	(3.284)
304.97	0.874	(1.579)	0.988	(1.674)	1.092	(1.756)	1.209	(1.904)	1.319	(2.213)	1.432	(2.856)	1.545	(3.496)
359.97	1.016	(1.360)	1.143	(1.886)	1.263	(2.853)	1.392	(3.759)	1.524	(4.158)	1.652	(4.083)	1.788	(3.931)
442.47	1.231	4.068	1.381	3.915	1.537	3.748	1.692	3.620	1.846	3.517	2.006	3.404	2.155	3.389
524.97	1.470	3.775	1.640	3.672	1.822	3.525	2.012	3.409	2.211	3.288	2.394	3.196	2.592	3.196
699.97	1.964	3.332	2.203	3.242	2.449	3.141	2.712	3.077	2.952	3.016	3.207	2.928	3.471	2.949
869.97	2.464	3.198	2.778	3.137	3.092	3.024	3.442	2.971	3.716	2.922	4.062	2.878	4.381	2.912
949.97	2.813	3.273	3.135	3.191	3.496	3.139	3.850	3.065	4.208	3.046	4.586	2.993	4.965	2.988
1009.97	2.998	3.045	3.352	2.979	3.758	2.911	4.163	2.859	4.499	2.815	4.902	2.756	5.298	2.775
1064.97	3.104	2.742	3.492	2.670	3.903	2.613	4.293	2.576	4.685	2.546	5.088	2.492	5.495	2.454
	$\times 10^6$	$\times 10^{-3}$	$\times 10^6$	$\times 10^{-3}$	$\times 10^6$	$\times 10^{-3}$	$\times 10^6$	$\times 10^{-3}$	$\times 10^6$	$\times 10^{-3}$	$\times 10^6$	$\times 10^{-3}$	$\times 10^6$	$\times 10^{-3}$

Table C2: C_f data for case of $d_T = 0.1\,mm$ trip wire. Bracketed values indicated a laminar boundary layer and values are provided for qualitative assessment only.

x (mm)	$U_\infty = 40\,\mathrm{m/s}$		45		50		55		60		65		70	
	Re_x	C_f	Re_x	C_f	Re_x	C_f	Re_x	C_f	Re_x	C_f	Re_x	C_f	Re_x	C_f
304.97	0.872	(1.636)	0.982	3.541	1.093	3.462	1.203	3.371	1.313	3.211	1.426	3.139	1.541	3.146
359.97	1.006	(2.621)	1.130	3.363	1.259	3.256	1.381	3.140	1.515	3.016	1.649	2.951	1.778	2.974
442.47	1.222	3.984	1.375	3.476	1.533	3.091	1.693	3.043	1.837	2.883	1.996	2.826	2.162	2.760
	$\times 10^6$	$\times 10^{-3}$	$\times 10^6$	$\times 10^{-3}$	$\times 10^6$	$\times 10^{-3}$	$\times 10^6$	$\times 10^{-3}$	$\times 10^6$	$\times 10^{-3}$	$\times 10^6$	$\times 10^{-3}$	$\times 10^6$	$\times 10^{-3}$

Table C3: C_f data for case of $d_T = 0.2\,mm$ trip wire.

x (mm)	$U_\infty = 40\,\mathrm{m/s}$		45		50		55		60		65		70	
	Re_x	C_f	Re_x	C_f	Re_x	C_f	Re_x	C_f	Re_x	C_f	Re_x	C_f	Re_x	C_f
73.07	0.207	6.655	0.233	6.292	0.259	6.157	0.285	5.937	0.311	5.744	0.339	5.560	0.363	5.415
78.70	0.225	6.542	0.253	6.171	0.281	6.052	0.310	5.845	0.340	5.670	0.368	5.523	0.396	5.376
84.34	0.243	5.816	0.272	5.676	0.303	5.665	0.336	5.520	0.359	5.441	0.399	5.290	0.432	5.158
89.97	0.260	5.748	0.292	5.676	0.327	5.580	0.358	5.431	0.390	5.295	0.429	5.173	0.457	5.065
112.47	0.331	4.994	0.372	4.892	0.413	4.749	0.455	4.779	0.497	4.664	0.542	4.568	0.580	4.467
134.97	0.396	4.714	0.447	4.499	0.500	4.390	0.549	4.433	0.603	4.326	0.651	4.241	0.706	4.134
157.47	0.464	4.332	0.524	4.202	0.581	4.109	0.641	4.025	0.707	4.052	0.759	3.970	0.821	3.877
179.97	0.531	4.143	0.594	4.007	0.663	3.907	0.728	3.829	0.799	3.868	0.872	3.771	0.935	3.686
214.97	0.631	3.859	0.713	3.753	0.793	3.693	0.866	3.619	0.950	3.570	1.031	3.598	1.111	3.512
249.97	0.731	3.695	0.820	3.608	0.914	3.522	1.005	3.451	1.093	3.395	1.197	3.415	1.296	3.344
304.97	0.873	3.397	0.979	3.307	1.092	3.247	1.204	3.167	1.318	3.118	1.426	3.075	1.538	3.089
359.97	1.003	3.184	1.134	3.113	1.264	3.047	1.389	2.989	1.514	2.931	1.651	2.890	1.781	2.832
524.97	1.453	3.055	1.631	2.991	1.822	2.927	2.002	2.878	2.189	2.840	2.388	2.780	2.556	2.746
699.97	1.950	2.915	2.192	2.874	2.433	2.821	2.685	2.773	2.939	2.728	3.204	2.688	3.432	2.667
869.97	2.457	2.951	2.777	2.899	3.083	2.841	3.403	2.802	3.708	2.770	4.033	2.715	4.371	2.679
949.97	2.775	3.098	3.125	3.052	3.494	2.970	3.840	2.920	4.195	2.908	4.564	2.857	4.944	2.888
1009.97	2.954	2.879	3.337	2.792	3.723	2.756	4.087	2.708	4.489	2.668	4.758	2.650	5.241	2.585
1064.97	3.093	2.574	3.487	2.530	3.884	2.484	4.271	2.431	4.663	2.408	5.074	2.379	5.452	2.342
	$\times 10^6$	$\times 10^{-3}$	$\times 10^6$	$\times 10^{-3}$	$\times 10^6$	$\times 10^{-3}$	$\times 10^6$	$\times 10^{-3}$	$\times 10^6$	$\times 10^{-3}$	$\times 10^6$	$\times 10^{-3}$	$\times 10^6$	$\times 10^{-3}$

Table C4: C_f data for case of $d_T = 0.5\,mm$ trip wire.

x (mm)	$U_\infty = 40\,\text{m/s}$		45		50		55		60		65		70	
	Re_x	C_f	Re_x	C_f	Re_x	C_f	Re_x	C_f	Re_x	C_f	Re_x	C_f	Re_x	C_f
73.07	0.204	1.669	0.232	2.685	0.257	3.017	0.285	3.176	0.311	3.250	0.339	3.246	0.369	3.278
78.70	0.226	5.268	0.251	5.102	0.282	4.967	0.311	4.970	0.339	4.803	0.369	4.636	0.396	4.512
84.34	0.243	5.459	0.273	5.283	0.304	5.137	0.336	5.117	0.367	4.959	0.396	4.821	0.429	4.697
89.97	0.264	5.307	0.298	5.182	0.331	5.081	0.365	5.065	0.398	4.954	0.432	4.859	0.468	4.711
112.47	0.331	5.038	0.372	4.924	0.414	4.841	0.455	4.874	0.499	4.752	0.541	4.664	0.586	4.568
134.97	0.399	4.827	0.449	4.709	0.498	4.630	0.549	4.657	0.600	4.570	0.653	4.476	0.706	4.367
157.47	0.463	4.247	0.522	4.137	0.581	4.089	0.641	4.012	0.699	4.050	0.760	3.952	0.824	3.873
179.97	0.529	3.906	0.595	3.827	0.665	3.757	0.731	3.688	0.800	3.730	0.867	3.664	0.941	3.568
214.97	0.632	3.691	0.712	3.609	0.791	3.556	0.870	3.503	0.953	3.442	1.023	3.479	1.128	3.378
249.97	0.730	3.571	0.821	3.495	0.914	3.408	1.008	3.360	1.105	3.304	1.194	3.355	1.296	3.260
304.97	0.872	3.335	0.978	3.262	1.092	3.188	1.210	3.131	1.324	3.090	1.429	3.027	1.564	3.035
359.97	1.005	3.138	1.134	3.068	1.262	3.022	1.393	2.942	1.531	2.885	1.652	2.841	1.779	2.804
524.97	1.456	3.008	1.633	2.936	1.824	2.893	2.011	2.833	2.192	2.764	2.382	2.735	2.576	2.711
699.97	1.949	2.925	2.196	2.858	2.437	2.816	2.694	2.763	2.942	2.725	3.195	2.702	3.505	2.645
869.97	2.472	2.963	2.777	2.874	3.084	2.816	3.404	2.789	3.740	2.726	4.047	2.704	4.383	2.660
949.97	2.776	3.089	3.139	3.038	3.490	2.977	3.847	2.913	4.200	2.902	4.568	2.862	4.981	2.870
1009.97	2.972	2.865	3.347	2.780	3.719	2.750	4.107	2.705	4.485	2.655	4.872	2.634	5.306	2.650
1064.97	3.097	2.604	3.492	2.538	3.879	2.502	4.283	2.458	4.667	2.430	5.090	2.383	5.490	2.345
	$\times 10^6$	$\times 10^{-3}$	$\times 10^6$	$\times 10^{-3}$	$\times 10^6$	$\times 10^{-3}$	$\times 10^6$	$\times 10^{-3}$	$\times 10^6$	$\times 10^{-3}$	$\times 10^6$	$\times 10^{-3}$	$\times 10^6$	$\times 10^{-3}$

Table C5: C_f data for case of 80 grit roughness strip.

| x (mm)	$U_\infty = 40\,\mathrm{m/s}$		45		50		55		60		65		70	
	Re_x	C_f	Re_x	C_f	Re_x	C_f	Re_x	C_f	Re_x	C_f	Re_x	C_f	Re_x	C_f
73.07	0.204	5.036	0.233	5.306	0.261	4.859	0.287	4.932	0.311	4.893	0.340	4.811	0.364	4.757
78.70	0.226	5.291	0.252	5.302	0.280	5.195	0.310	5.286	0.338	5.151	0.368	4.935	0.398	4.801
84.34	0.243	5.373	0.272	5.294	0.304	5.189	0.338	5.193	0.364	5.075	0.396	4.881	0.431	4.799
89.97	0.260	5.356	0.293	5.141	0.326	5.029	0.357	5.054	0.392	4.949	0.427	4.781	0.463	4.638
112.47	0.330	4.953	0.372	4.791	0.413	4.723	0.456	4.737	0.498	4.625	0.542	4.519	0.586	4.431
134.97	0.398	4.496	0.449	4.379	0.497	4.284	0.548	4.227	0.599	4.243	0.651	4.147	0.706	4.049
157.47	0.462	4.287	0.522	4.155	0.580	4.085	0.638	4.013	0.701	4.048	0.760	3.965	0.821	3.859
179.97	0.531	4.043	0.594	3.944	0.665	3.873	0.733	3.811	0.799	3.846	0.866	3.770	0.938	3.677
214.97	0.631	3.853	0.713	3.769	0.790	3.677	0.871	3.608	0.952	3.550	1.035	3.572	1.123	3.478
249.97	0.729	3.662	0.819	3.556	0.912	3.482	1.006	3.422	1.098	3.379	1.196	3.399	1.293	3.317
304.97	0.870	3.399	0.983	3.320	1.095	3.242	1.207	3.166	1.315	3.123	1.430	3.081	1.544	3.081
359.97	1.008	3.177	1.132	3.123	1.262	3.030	1.393	2.957	1.518	2.903	1.651	2.866	1.780	2.796
524.97	1.453	3.051	1.636	2.948	1.826	2.887	2.006	2.836	2.197	2.793	2.380	2.734	2.579	2.672
699.97	1.951	2.942	2.201	2.867	2.441	2.828	2.686	2.759	2.943	2.703	3.193	2.672	3.461	2.610
869.97	2.465	2.942	2.779	2.858	3.102	2.812	3.408	2.769	3.726	2.726	4.052	2.703	4.355	2.665
949.97	2.774	3.105	3.133	2.998	3.486	2.959	3.841	2.911	4.204	2.875	4.566	2.859	4.941	2.856
1009.97	2.960	2.886	3.336	2.804	3.717	2.754	4.094	2.704	4.479	2.661	4.878	2.634	5.261	2.673
1064.97	3.104	2.600	3.494	2.523	3.893	2.497	4.271	2.448	4.680	2.416	5.088	2.392	5.470	2.349
	$\times 10^6$	$\times 10^{-3}$	$\times 10^6$	$\times 10^{-3}$	$\times 10^6$	$\times 10^{-3}$	$\times 10^6$	$\times 10^{-3}$	$\times 10^6$	$\times 10^{-3}$	$\times 10^6$	$\times 10^{-3}$	$\times 10^6$	$\times 10^{-3}$

Appendix D   Pressure Coefficients
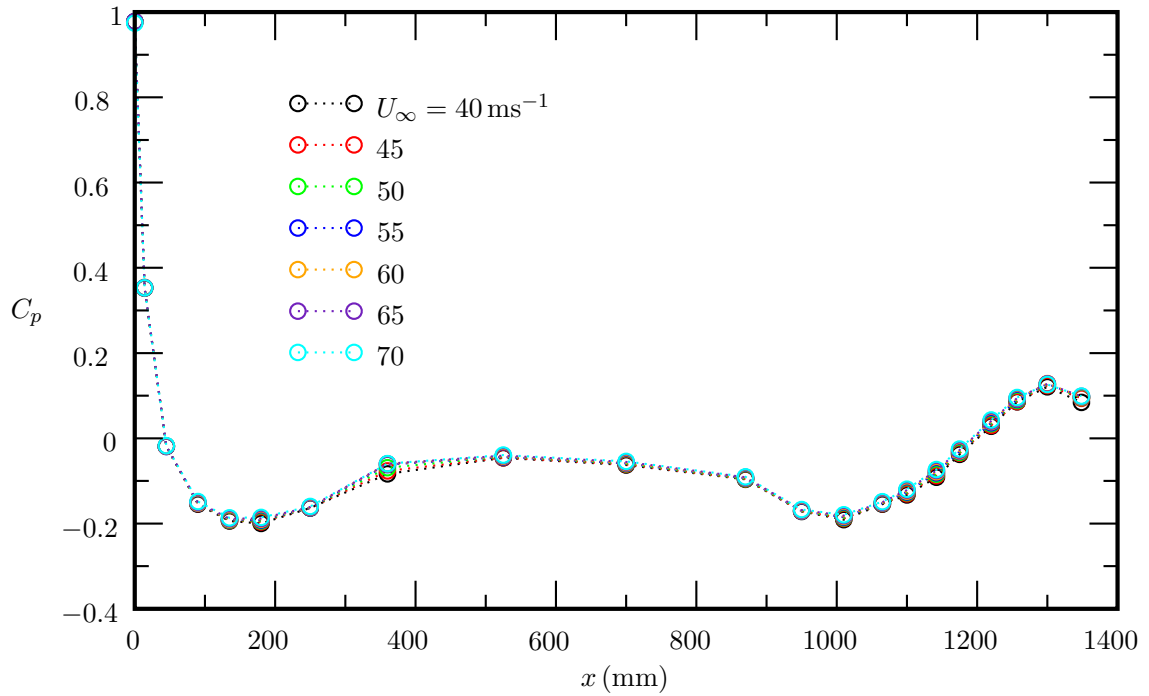
Figure D1: *Pressure coefficient across the range of free-stream velocities for the un-tripped case.*
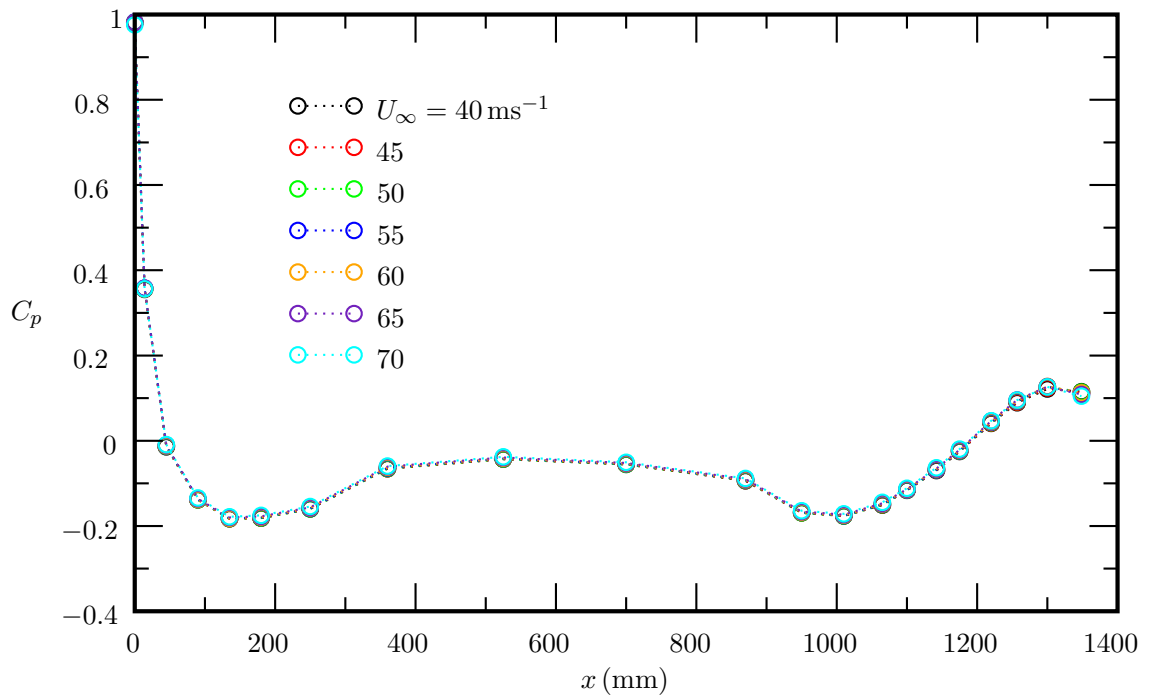

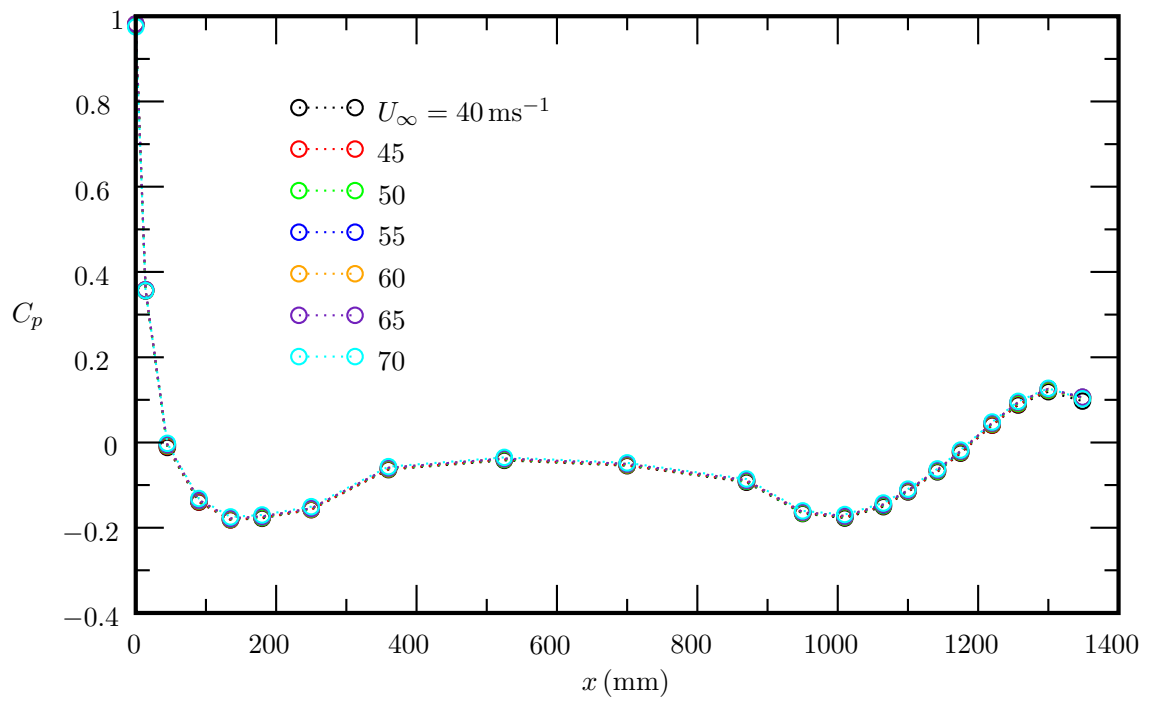**Figure D2:** *Pressure coefficient across the range of free-stream velocities for the trip wire $d_T = 0.5\,mm$ case.*

Figure D3: *Pressure coefficient across the range of free-stream velocities for the grit-80 trip case.*

Table D1: C_p *data for case of no trip device. The table also gives the* x *coordinates of the static pressure ports, where bracketed port numbers indicate the lateral ports which were not connected.*

x (mm)	Port No.	$U_\infty = 40\,\mathrm{m/s}$ C_p	45 C_p	50 C_p	55 C_p	60 C_p	65 C_p	70 C_p
0.0	1	0.9779	0.9762	0.9767	0.9775	0.9768	0.9777	0.9740
14.0	2	0.3520	0.3527	0.3538	0.3532	0.3537	0.3536	0.3530
45.0	3, (4, 5)	-0.0190	-0.0186	-0.0185	-0.0193	-0.0187	-0.0179	-0.0173
90.0	6	-0.1545	-0.1530	-0.1523	-0.1522	-0.1515	-0.1501	-0.1485
135.0	7	-0.1940	-0.1927	-0.1918	-0.1908	-0.1902	-0.1886	-0.1867
180.0	8	-0.1996	-0.1962	-0.1939	-0.1919	-0.1899	-0.1878	-0.1854
250.0	9, (10, 11)	-0.1634	-0.1634	-0.1631	-0.1631	-0.1623	-0.1611	-0.1600
360.0	12	-0.0834	-0.0764	-0.0690	-0.0618	-0.0605	-0.0598	-0.0592
525.0	13	-0.0459	-0.0452	-0.0434	-0.0435	-0.0423	-0.0406	-0.0394
700.0	14, (15, 16)	-0.0625	-0.0612	-0.0596	-0.0586	-0.0575	-0.0554	-0.0541
870.0	17	-0.0963	-0.0954	-0.0945	-0.0937	-0.0926	-0.0915	-0.0903
950.0	18, (19, 20)	-0.1717	-0.1709	-0.1704	-0.1706	-0.1697	-0.1684	-0.1670
1010.0	21, (22, 23)	-0.1910	-0.1882	-0.1865	-0.1849	-0.1833	-0.1814	-0.1792
1065.0	24	-0.1547	-0.1534	-0.1528	-0.1523	-0.1513	-0.1501	-0.1486
1100.0	25, (26, 27)	-0.1330	-0.1302	-0.1275	-0.1259	-0.1238	-0.1214	-0.1195
1142.0	28	-0.0913	-0.0878	-0.0840	-0.0808	-0.0785	-0.0755	-0.0731
1175.0	29	-0.0375	-0.0351	-0.0330	-0.0307	-0.0295	-0.0274	-0.0252
1220.0	30, (31, 32)	0.0283	0.0303	0.0342	0.0366	0.0390	0.0407	0.0429
1257.0	33	0.0856	0.0864	0.0890	0.0913	0.0932	0.0945	0.0958
1300.0	34	0.1209	0.1239	0.1265	0.1276	0.1284	0.1276	0.1265
1348.6	35	0.0842	0.0939	0.0958	0.0969	0.0970	0.0984	0.0991

Table D2: C_p data for case of $d_T = 0.2$ mm trip wire.

x (mm)	$U_\infty = 40$ m/s C_p	45 C_p	50 C_p	55 C_p	60 C_p	65 C_p	70 C_p
0	0.9799	0.9796	0.9814	0.9812	0.9812	0.9789	0.9741
14.0	0.3572	0.3561	0.3579	0.3590	0.3595	0.3568	0.3573
45.0	-0.0145	-0.0138	-0.0127	-0.0111	-0.0105	-0.0111	-0.0087
90.0	-0.1419	-0.1385	-0.1375	-0.1364	-0.1359	-0.1354	-0.1328
135.0	-0.1802	-0.1802	-0.1796	-0.1782	-0.1777	-0.1768	-0.1739
180.0	-0.1777	-0.1771	-0.1764	-0.1748	-0.1740	-0.1729	-0.1706
250.0	-0.1571	-0.1564	-0.1555	-0.1541	-0.1532	-0.1520	-0.1499
360.0	-0.0625	-0.0623	-0.0606	-0.0594	-0.0582	-0.0572	-0.0552
525.0	-0.0412	-0.0402	-0.0389	-0.0379	-0.0370	-0.0356	-0.0341
700.0	-0.0523	-0.0520	-0.0511	-0.0499	-0.0492	-0.0479	-0.0465
870.0	-0.0913	-0.0908	-0.0892	-0.0880	-0.0871	-0.0858	-0.0842
950.0	-0.1656	-0.1650	-0.1648	-0.1632	-0.1627	-0.1614	-0.1596
1010.0	-0.1751	-0.1746	-0.1736	-0.1723	-0.1712	-0.1699	-0.1680
1065.0	-0.1494	-0.1487	-0.1472	-0.1457	-0.1445	-0.1431	-0.1412
1100.0	-0.1138	-0.1134	-0.1126	-0.1112	-0.1101	-0.1092	-0.1077
1142.0	-0.0682	-0.0672	-0.0663	-0.0646	-0.0635	-0.0623	-0.0609
1175.0	-0.0223	-0.0220	-0.0212	-0.0198	-0.0189	-0.0181	-0.0169
1220.0	0.0431	0.0442	0.0445	0.0467	0.0474	0.0484	0.0495
1257.0	0.0917	0.0928	0.0932	0.0951	0.0957	0.0972	0.0984
1300.0	0.1210	0.1239	0.1257	0.1264	0.1272	0.1277	0.1295
1348.6	0.1089	0.1130	0.1149	0.1152	0.1139	0.1122	0.1102

Table D3: C_p data for case of $d_T = 0.5$ mm trip wire.

x (mm)	$U_\infty = 40$ m/s C_p	45 C_p	50 C_p	55 C_p	60 C_p	65 C_p	70 C_p
0.0	0.9803	0.9801	0.9817	0.9824	0.9808	0.9805	0.9757
14.0	0.3550	0.3563	0.3571	0.3578	0.3570	0.3579	0.3563
45.0	-0.0144	-0.0126	-0.0131	-0.0122	-0.0117	-0.0099	-0.0089
90.0	-0.1384	-0.1380	-0.1389	-0.1379	-0.1377	-0.1361	-0.1341
135.0	-0.1826	-0.1833	-0.1831	-0.1822	-0.1819	-0.1801	-0.1782
180.0	-0.1816	-0.1811	-0.1813	-0.1800	-0.1791	-0.1772	-0.1750
250.0	-0.1600	-0.1591	-0.1600	-0.1587	-0.1577	-0.1563	-0.1542
360.0	-0.0658	-0.0653	-0.0651	-0.0637	-0.0623	-0.0606	-0.0593
525.0	-0.0433	-0.0428	-0.0429	-0.0415	-0.0409	-0.0392	-0.0377
700.0	-0.0555	-0.0552	-0.0556	-0.0541	-0.0536	-0.0523	-0.0505
870.0	-0.0939	-0.0934	-0.0930	-0.0919	-0.0912	-0.0898	-0.0883
950.0	-0.1690	-0.1688	-0.1692	-0.1679	-0.1674	-0.1661	-0.1641
1010.0	-0.1763	-0.1762	-0.1768	-0.1755	-0.1747	-0.1735	-0.1714
1065.0	-0.1510	-0.1502	-0.1501	-0.1489	-0.1481	-0.1467	-0.1443
1100.0	-0.1165	-0.1159	-0.1160	-0.1155	-0.1145	-0.1135	-0.1115
1142.0	-0.0698	-0.0690	-0.0683	-0.0678	-0.0664	-0.0653	-0.0634
1175.0	-0.0253	-0.0246	-0.0245	-0.0236	-0.0223	-0.0212	-0.0196
1220.0	0.0408	0.0414	0.0424	0.0434	0.0449	0.0464	0.0471
1257.0	0.0891	0.0905	0.0922	0.0927	0.0942	0.0956	0.0955
1300.0	0.1214	0.1237	0.1263	0.1270	0.1274	0.1266	0.1262
1348.6	0.1153	0.1132	0.1141	0.1111	0.1121	0.1085	0.1046

Table D4: C_p data for case of grit-80.

x (mm)	$U_\infty = 40\,\text{m/s}$ C_p	45 C_p	50 C_p	55 C_p	60 C_p	65 C_p	70 C_p
0.0	0.9794	0.9815	0.9798	0.9820	0.9815	0.9815	0.9750
14.0	0.3553	0.3562	0.3571	0.3584	0.3583	0.3583	0.3559
45.0	-0.0117	-0.0094	-0.0075	-0.0052	-0.0048	-0.0048	-0.0021
90.0	-0.1402	-0.1391	-0.1371	-0.1357	-0.1349	-0.1349	-0.1315
135.0	-0.1818	-0.1812	-0.1800	-0.1787	-0.1781	-0.1781	-0.1747
180.0	-0.1780	-0.1764	-0.1759	-0.1741	-0.1735	-0.1735	-0.1701
250.0	-0.1577	-0.1573	-0.1561	-0.1545	-0.1545	-0.1545	-0.1507
360.0	-0.0637	-0.0627	-0.0618	-0.0597	-0.0593	-0.0593	-0.0567
525.0	-0.0419	-0.0401	-0.0399	-0.0381	-0.0376	-0.0376	-0.0349
700.0	-0.0545	-0.0533	-0.0526	-0.0507	-0.0500	-0.0500	-0.0477
870.0	-0.0934	-0.0914	-0.0911	-0.0893	-0.0884	-0.0884	-0.0858
950.0	-0.1668	-0.1652	-0.1655	-0.1639	-0.1633	-0.1633	-0.1604
1010.0	-0.1772	-0.1754	-0.1750	-0.1734	-0.1722	-0.1722	-0.1692
1065.0	-0.1507	-0.1487	-0.1482	-0.1463	-0.1450	-0.1450	-0.1420
1100.0	-0.1161	-0.1149	-0.1142	-0.1127	-0.1120	-0.1120	-0.1094
1142.0	-0.0688	-0.0671	-0.0670	-0.0651	-0.0641	-0.0641	-0.0619
1175.0	-0.0251	-0.0234	-0.0223	-0.0208	-0.0198	-0.0198	-0.0180
1220.0	0.0403	0.0415	0.0433	0.0454	0.0461	0.0461	0.0479
1257.0	0.0878	0.0902	0.0916	0.0942	0.0948	0.0948	0.0963
1300.0	0.1191	0.1220	0.1227	0.1260	0.1257	0.1257	0.1272
1348.6	0.0972	0.1049	0.1042	0.1062	0.1056	0.1056	0.1023

DEFENCE SCIENCE AND TECHNOLOGY ORGANISATION DOCUMENT CONTROL DATA			1. CAVEAT/PRIVACY MARKING	

2. TITLE Skin-Friction Measurements on a Model Submarine	3. SECURITY CLASSIFICATION Document (U) Title (U) Abstract (U)

4. AUTHORS M. B. Jones, L. P. Erm, A. Valiyff and S. M. Henbest	5. CORPORATE AUTHOR Defence Science and Technology Organisation 506 Lorimer St, Fishermans Bend, Victoria 3207, Australia

6a. DSTO NUMBER DSTO–TR–2898	6b. AR NUMBER AR 015-744	6c. TYPE OF REPORT Technical Report	7. DOCUMENT DATE October, 2013

8. FILE NUMBER	9. TASK NUMBER ERP07/299	10. TASK SPONSOR CDS	11. No. OF PAGES 46	12. No. OF REFS 0

13. URL OF ELECTRONIC VERSION http://www.dsto.defence.gov.au/ publications/scientific.php	14. RELEASE AUTHORITY Chief, Aerospace Division

15. SECONDARY RELEASE STATEMENT OF THIS DOCUMENT

Approved for Public Release

OVERSEAS ENQUIRIES OUTSIDE STATED LIMITATIONS SHOULD BE REFERRED THROUGH DOCUMENT EXCHANGE, PO BOX 1500, EDINBURGH, SOUTH AUSTRALIA 5111

16. DELIBERATE ANNOUNCEMENT

No Limitations

17. CITATION IN OTHER DOCUMENTS

No Limitations

18. DSTO RESEARCH LIBRARY THESAURUS

Submarines
Skin friction
Turbulent boundary layer
Modelling
Fluid dynamics

19. ABSTRACT

Experimental skin-friction and pressure-coefficient data for a generic scale-model submarine, tested in the Low-Speed Wind Tunnel at DSTO, are presented. The effect on skin-friction and pressure coefficients due to different sizes and types of boundary layer tripping devices, including the case of no tripping device, was investigated for the Reynolds number range of 3.58×10^6 to 6.27×10^6, where the Reynolds number is based on model length. Skin friction was measured using the Preston-tube method which is a technique applicable to turbulent boundary layers only. For the laminar and transition regions the Preston tube only provided qualitative results. The results demonstrate the importance of correctly tripping the boundary layer and provide a guide on determining the size and type of tripping device required to achieve a correctly stimulated turbulent boundary layer for a given tunnel free-stream velocity. While the results are specific to the model geometry tested and for the given trip location, the methodology is applicable to other general model geometries and trip locations. This report does not address the difficult problem of where to place the trip.